

1 **Recombinant rotaviruses rescued by reverse genetics**
2 **reveal the role of NSP5 hyperphosphorylation in the**
3 **assembly of viral factories**

4

5 Guido Papa^{1,*}, Luca Venditti¹, Francesca Arnoldi^{1,2}, Elisabeth M. Schraner³,
6 Christiaan Potgieter^{4,5}, Alexander Borodavka⁶, Catherine Eichwald³ and Oscar R.
7 Burrone^{1,*}

8

9 ¹ International Centre for Genetic Engineering and Biotechnology, ICgeb, Padriciano 99, 34149
10 Trieste, Italy

11 ² Department of Medicine, Surgery and Health Sciences, University of Trieste, Trieste, Italy

12 ³ Institute of Virology, University of Zürich, Zürich, Switzerland

13 ⁴ Department of Biochemistry, Centre for Human Metabolomics, North-West University,
14 Potchefstroom, South Africa

15 ⁵ Deltamune (Pty) Ltd, 248 Jean Avenue, Lyttelton, Centurion, South Africa

16 ⁶ Astbury Centre for Structural Molecular Biology, School of Molecular and Cellular Biology,
17 University of Leeds, Leeds, UK

18

19

20

21 * Corresponding authors, guido.papa@icgeb.org, burrone@icgeb.org

22

23

24

25

26

27

28

29

30

31

32

33

34

35

36 **ABSTRACT**

37 Rotavirus (RV) replicates in round-shaped cytoplasmic viral factories although
38 how they assemble remains unknown.

39 During RV infection, NSP5 undergoes hyperphosphorylation, which is primed by
40 the phosphorylation of a single serine residue. The role of this post-translational
41 modification in the formation of viroplasms and its impact on the virus replication
42 remains obscure. Here we investigated the role of NSP5 during RV infection by
43 taking advantage of a modified fully tractable reverse genetics system. An NSP5
44 trans-complementing cell line was used to generate and characterise several
45 recombinant rotaviruses (rRVs) with mutations in NSP5. We demonstrate that a
46 rRV lacking NSP5, was completely unable to assemble viroplasms and to
47 replicate, confirming its pivotal role in rotavirus replication.

48 A number of mutants with impaired NSP5 phosphorylation were generated to
49 further interrogate the function of this post-translational modification in the
50 assembly of replication-competent viroplasms. We showed that the rRV mutant
51 strains exhibit impaired viral replication and the ability to assemble round-shaped
52 viroplasms in MA104 cells. Furthermore, we have investigated the mechanism of
53 NSP5 hyper-phosphorylation during RV infection using NSP5 phosphorylation-
54 negative rRV strains, as well as MA104-derived stable transfectant cell lines
55 expressing either wt NSP5 or selected NSP5 deletion mutants. Our results
56 indicate that NSP5 hyper-phosphorylation is a crucial step for the assembly of
57 round-shaped viroplasms, highlighting the key role of the C-terminal tail of NSP5
58 in the formation of replication-competent viral factories. Such a complex NSP5
59 phosphorylation cascade may serve as a paradigm for the assembly of functional
60 viral factories in other RNA viruses.

61
62
63
64
65
66

67 **IMPORTANCE**

68 Rotavirus (RV) double-stranded RNA genome is replicated and packaged into
69 virus progeny in cytoplasmic structures termed viroplasms. The non-structural
70 protein NSP5, which undergoes a complex hyperphosphorylation process during
71 RV infection, is required for the formation of these virus-induced organelles.
72 However, its roles in viroplasm formation and RV replication have never been
73 directly assessed due to the lack of a fully tractable reverse genetics (RG)
74 system for rotaviruses. Here we show a novel application of a recently developed
75 RG system by establishing a stable trans-complementing NSP5-producing cell
76 line required to rescue rotaviruses with mutations in NSP5. This approach
77 allowed us to provide the first direct evidence of the pivotal role of this protein
78 during RV replication. Furthermore, using recombinant RV mutants we shed light
79 on the molecular mechanism of NSP5 hyperphosphorylation during infection and
80 its involvement in the assembly and maturation of replication-competent
81 viroplasms.

82

83

84

85

86

87

88

89

90

91

92

93

94

95

96

97

98 INTRODUCTION

99 Rotavirus (RV) is the most common cause of viral gastroenteritis in young
100 children and infants worldwide (1, 2). It is a non-enveloped RNA virus with a
101 genome composed of 11 segments of double-stranded RNA (dsRNA), which
102 replicates in cytoplasmic structures primarily composed of viral proteins (3–5).
103 During infection, the first steps of viral morphogenesis and genome replication
104 occur within cytoplasmic viral replication factories known as viroplasms. (3, 5–7).
105 The assembly of viroplasms requires co-expression of at least two non-structural
106 proteins, NSP5 and NSP2 (8, 9), however, how these virus-induced organelles
107 are formed remains unknown.

108 Other viral proteins also found in viroplasms include RNA-dependent RNA
109 polymerase (RdRp) VP1, the main inner-core protein VP2, guanylttransferase/
110 methylase VP3, and the middle layer (inner capsid) protein VP6 (10, 11).
111 Biochemical evidence suggests that viroplasms are essential for RV replication
112 since the virus production is highly impaired upon silencing of either NSP2 or
113 NSP5 (12–15).

114 Rotavirus NSP5, encoded by genome segment 11, is a small serine (Ser)- and
115 threonine (Thr)-rich non-structural protein that undergoes multiple post-
116 translational modifications in virus-infected cells, including O-linked glycosylation
117 (16), N-acetylation (17), SUMOylation (18) and crucially hyperphosphorylation
118 that involves several distinct Ser residues (19, 20). The NSP5
119 hyperphosphorylation is a complex process, which gives rise to multiple
120 phosphorylation states ranging from the most abundant 28 kDa phospho-isoform,
121 up to the hyperphosphorylated 32-34 kDa states (19, 20). All these forms have
122 been found to be more stable in viroplasms, while chemical disruption of
123 viroplasms results in NSP5 de-phosphorylation (21). The mechanism of NSP5
124 phosphorylation is not yet wholly understood, but it involves interactions with
125 other viral proteins. When expressed alone in non-infected cells, NSP5 is not
126 phosphorylated, while co-expression with NSP2 or VP2 results in NSP5
127 hyperphosphorylation and formation of viroplasm-like structures (VLS) (8, 22,
128 23). NSP5 hyperphosphorylation involves the phosphorylation of Serine 67

129 (Ser67) by Casein Kinase 1 α (CK1 α) to initiate the phosphorylation cascade (24,
130 25) and it is considered to be essential for the assembly of viroplasms (26).
131 Although the structure of NSP5 remains unknown, it readily forms higher
132 molecular weight oligomeric species in solution, potentially providing a larger
133 interface for interacting with multiple components of viroplasms (27).
134 In addition, the C-terminal region ('a tail' including amino acids 180-198) is
135 required for NSP5 decamerisation *in vitro* (27) and VLS formation *in vivo* (7).
136 However, due to the lack of a fully tractable reverse genetics (RG) system for
137 RVs until recently, previous studies on NSP5 have been carried out using the
138 mutants expressed in the absence of a complete set of viral proteins. Here, we
139 took advantage of the novel plasmid only-based, helper-virus free RG systems
140 for rotaviruses (28, 29) to gain new insights into the mechanisms of NSP5
141 hyperphosphorylation and its role in viroplasm assembly and virus replication
142 during viral infection.
143 To achieve this, we generated and characterised several viable recombinant
144 rotaviruses (rRVs) with mutations in NSP5. Using these mutants, we show the
145 role of NSP5 hyperphosphorylation for viroplasm assembly and in genome
146 replication. These studies shed light on a complex hierarchical mechanism of
147 NSP5 hyperphosphorylation during rotaviral infection.

148

149 **MATERIALS AND METHODS**

150

151 **Cells and viruses.** MA104 (embryonic African green monkey kidney cells, ATCC
152 CRL-2378.1 from *Chlorocebus aethiops*), U2OS (Human bone osteosarcoma
153 epithelial cells), Caco-2 (colorectal adenocarcinoma human intestinal epithelial
154 cell line, ATCC®HTB-37) and HEK293T (embryonic human kidney epithelial,
155 ATCC®CRL-3216) cells were cultured in Dulbecco's Modified Eagle's Medium
156 (DMEM) (Life Technologies) supplemented with 10% Fetal Bovine Serum (FBS)
157 (Life Technologies) and 50 μ g/ml gentamycin (Biochrom AG).

158 MA104-NSP5-EGFP cells (MA-NSP5-EGFP) (7) were cultured in DMEM
159 supplemented with 10% FBS (Life Technologies), 50 µg/ml gentamycin
160 (Biochrom AG) and 1 mg/ml geneticin (Gibco-BRL, Life Technologies).

161 MA104-NSP2-mCherry (MA-NSP2-mCherry), MA104-Δ3 (MA-Δ3), MA104-Δtail
162 (MA-ΔT) and MA104-NSP5wt (MA-NSP5) stable transfectant cell lines
163 (embryonic African green monkey kidney cells, ATCC® CRL-2378) were grown
164 in DMEM (Life Technologies) containing 10% FBS, 50 µg/ml gentamycin
165 (Biochrom AG) and 5 µg/ml puromycin (Sigma-Aldrich).

166 BHK-T7 cells (Baby hamster kidney stably expressing T7 RNA polymerase) were
167 cultured in Glasgow medium supplemented with 5% FBS, 10% Tryptose
168 Phosphate Broth (TPB) (Sigma-Aldrich), 50 µg/ml gentamycin (Biochrom AG),
169 2% Non-Essential Amino Acid (NEAA), 1% Glutamine.

170 Recombinant simian RV strain SA11 (rRV-wt), rescued using reverse genetics
171 system using cDNA clones encoding the wild-type SA11 (G3P[2]) virus (28), was
172 propagated in MA104 cells cultured in DMEM supplemented with 0.5 µg/ml
173 trypsin (Sigma Aldrich).

174

175 **Recombinant RVs Titration**

176 Recombinant NSP5 mutant RVs were grown in MA-NSP5 cells and the lysate
177 was 2-fold serially diluted and used to infect MA-NSP5 cells, seeded in 24-wells
178 plates with coverslips. After 1 hour of adsorption, virus was removed, and cells
179 were incubated at 37°C. At 5 hours post-infection (hpi), cells were fixed with 4%
180 paraformaldehyde (PFA) in phosphate buffer saline (PBS) [137 mM NaCl; 2.7
181 mM KCl; 8.1 mM Na₂HPO₄ and 1.74 mM KH₂PO₄ pH7.5] for 15 min at room
182 temperature and permeabilized for 5 min with PBS containing 0.01% Triton X-
183 100. Next, cells were incubated for 30 min with PBS supplemented with 1%
184 bovine serum albumin (PBS-BSA) at room temperature and then with anti-NSP5
185 (1:1000) or anti-VP2 (1:200) or anti-NSP2 (1:200) guinea pig serum diluted in
186 PBS-BSA. After washing three times with PBS, cells were incubated for 1 h at
187 room temperature with TRITC-conjugated Anti-guinea Pig IgG (Jackson
188 ImmunoResearch) (1:500) diluted in PBS-BSA.

189 Nuclei were stained with ProLong™ Diamond Antifade Mountant with DAPI
190 (Thermo Scientific). Samples were imaged using a confocal setup (Zeiss
191 Airyscan equipped with a 63x, NA=1.3 objective). Each viroplasms-containing
192 cell was counted as one focus-forming unit (FFU). The average of cells with
193 viroplasms of six fields of view per each virus dilution was determined and the
194 total number of cells containing viroplasms in the whole preparation was
195 estimated. The virus titre was determined as:

$$196 \quad \text{Virus Titer} \left(\frac{\text{FFU}}{\text{ml}} \right) = \frac{N * \text{Dilution Factor}}{V(\text{ml})}$$

197 where N is a total number of cells containing 1 or more viroplasms, and V is the
198 volume of virus inoculum added.

199

200 **Replication Kinetics of recombinant viruses**

201 MA104 cell line (ATCC CRL-2378.1) or stably transfected MA104 cells (NSP5;
202 $\Delta 3$, ΔT) were seeded into 24-well plates and subsequently infected with
203 recombinant RVs at MOI (FFU/cell) of 0.5 for multi-step growth curve
204 experiments and MOI 5 for a single-step growth curve experiment. After
205 adsorption for 1 h at 37°C, cells were washed twice with PBS and the medium
206 replaced with DMEM without trypsin. After incubation at 37°C, cells were
207 harvested after 8, 16, 24, 36 hours post virus adsorption. The cell lysates were
208 freeze-thawed three times and activated with trypsin (1 $\mu\text{g/ml}$) for 30 min at 37°C.
209 The lysates were used to infect monolayers of MA-NSP5 cells seeded in μ -Slide
210 8 Well Chamber Slide-well (iBidi GmbH, Munich, Germany). The cells were then
211 fixed 5 hours post infection for 15 min with 4% paraformaldehyde and
212 permeabilized for 5 min with PBS containing 0.01% Triton X-100. Next, cells
213 were incubated for 30 min with PBS-BSA at room temperature and then with anti-
214 NSP5 serum (1:1000) diluted in PBS-BSA. After three washes with PBS, cells
215 were incubated for 1 h at room temperature with TRITC-conjugated Anti-guinea
216 Pig IgG (Jackson ImmunoResearch) (1:500) diluted in PBS containing 1% BSA
217 (PBS-BSA).

218 The number of infected cells was counted, and the virus titres were expressed in
219 Focus-Forming Units per mL (FFU/mL).

220

221 **Plasmid construction.**

222 RV plasmids pT₇-VP1-SA11, pT₇-VP2-SA11, pT₇-VP3-SA11, pT₇-VP4-SA11,
223 pT₇-VP6-SA11, pT₇-VP7-SA11, pT₇-NSP1-SA11, pT₇-NSP2-SA11, pT₇-NSP3-
224 SA11, pT₇-NSP4-SA11, and pT₇-NSP5-SA11 (28) were used to rescue
225 recombinant RVs by reverse genetics. pT₇-NSP5/S67A carrying a mutation in the
226 nucleotide T220G in the gs11 and pT₇-NSP5/Tyr18Stop harbouring a nucleotide
227 substitution T75G were generated by QuikChange II Site-Directed Mutagenesis
228 (Agilent Technologies). pT₇-NSP5/ΔT was generated from pT₇-NSP5-SA11 by
229 deleting the last 18 C-terminal amino acids (FALRMRMKQVAMQLIEDL) using
230 substitution of the F181 encoding triplet with a stop codon. pT₇-NSP5/Δ176-180
231 were obtained deleting the amino acids 176 to 180 (YKKKY). The described
232 deletions were performed using the QuikChange II Site-Directed Mutagenesis kit
233 (Agilent Technologies).

234 For the generation of lentiviral plasmids, NSP5 and NSP2-mCherry were
235 amplified by PCR and inserted into the plasmid pAIP (Addgene #74171; (30) at
236 the *NotI-EcoRI* restriction enzymes sites to yield pAIP-NSP5 and pAIP-NSP2-
237 mCherry, which were then used to generate lentiviruses for the MA104-stable
238 transfectant cell lines (MA-NSP5 and MA-NSP2-mCherry) (31). NSP5/ΔT was
239 amplified from the pT₇-NSP5/ΔT by PCR and inserted into the pPB-MCS (Vector
240 Builder) at restriction enzyme sites *NheI-BamHI* to generate pPB-NSP5/ΔT for
241 the production of the stable transfectant MA-ΔT.

242 pPB-NSP5/Δ3, for MA-Δ3 stable cell line establishment, was generated with a
243 GenParts™ DNA Fragment (GenScript) containing NSP5 ORF lacking the amino
244 acids 80-130 (VKTNADAGVSMDSSAQSRPSSNVGCDQVDFSLNKG
245 LKVKANLDSSISIST) and inserted into the *NheI-BamHI* restriction sites of pPB-
246 MCS vector.

247

248 **Generation of stable cell lines**

249 MA-NSP5-EGFP were generated as previously described (7).
250 MA-NSP2-mCherry and MA-NSP5 cell line were generated using lentiviral vector
251 system (31). Briefly, HEK293T cells were maintained in DMEM (Life
252 Technologies) supplemented with 10% FBS (Life Technologies), and 50 µg/ml
253 gentamycin (Biochrom AG). Approximately 7×10^6 HEK293T cells were seeded
254 in 10 cm² tissue culture dishes 24 hours before transfection. For each well, 2.4
255 µg of pMD2-VSV-G, 4 µg of pMDLg pRRE, 1.8 µg of pRSV-Rev and 1.5 µg of
256 plasmid containing pAIP-NSP2-mCherry or pAIP-NSP5 and the human
257 immunodeficiency virus long terminal repeats were co-transfected with
258 Lipofectamine 3000 (Sigma-Aldrich) according to the manufacturer's instructions.
259 After 48 h, the virus was collected by filtration with a 0.45-µm polyvinylidene
260 fluoride filter and was immediately used or stored at -80 °C. For lentiviral
261 transduction, MA104 cells were transduced in six-well plates with 1 ml of lentiviral
262 supernatant for 2 days.
263 MA-Δ3 and MA-ΔT were generated using the PiggyBac Technology (32). Briefly,
264 10⁵ MA104 cells were transfected with the pCMV-HyPBase (32) and the
265 transposon plasmid pPB-NSP5/Δ3 and pPB-NSP5/ΔT using a ratio of 1:2.5 with
266 Lipofectamine 3000 (Sigma-Aldrich) according to the manufacturer's instructions.
267 The cells were maintained in DMEM supplemented with 10% FBS for 3 days and
268 then the cells were incubated with DMEM supplemented with 10% FBS and 5
269 µg/ml puromycin (Sigma-Aldrich) for 4 days to allow the selection of cells
270 expressing the gene of interest.

271

272 **Rescue of recombinant RVs (rRVs) from cloned cDNAs.**

273 To rescue recombinant RV strain SA11 (rRV-WT), monolayers of BHK-T7 cells
274 (4×10^5) cultured in 12-well plates were co-transfected using 2.5 µL of TransIT-
275 LT1 transfection reagent (Mirus) per microgram of DNA plasmid. Each mixture
276 comprised 0.8 µg of SA11 rescue plasmids: pT₇-VP1, pT₇-VP2, pT₇-VP3, pT₇-
277 VP4, pT₇-VP6, pT₇-VP7, pT₇-NSP1, pT₇-NSP3, pT₇-NSP4, and 2.4 µg of pT₇-
278 NSP2 and pT₇-NSP5 (29). Furthermore 0.8 µg of pcDNA3-NSP2 and 0.8 µg of

279 pcDNA3-NSP5, encoding NSP2 and NSP5 proteins, were also co-transfected to
280 increase rescue efficiency.

281 To rescue recombinant rRVs encoding NSP5 mutants, pT₇ plasmids encoding
282 NSP5/S67A, NSP5/Y18Stop, NSP5/Δ180-198 segments were used instead of
283 pT₇-NSP5. At 24 h post-transfection, MA-NSP5 cells (5×10^4 cells) were added
284 to transfected cells to provide a functional NSP5 for the virus rescue. The cells
285 were co-cultured for 3 days in FBS-free medium supplemented with trypsin (0.5
286 μg/mL) (Sigma Aldrich). After incubation, transfected cells were lysed by freeze-
287 thawing and 200 μl of the lysate was transferred to fresh MA-NSP5 cells. After
288 adsorption at 37°C for 1 hour, cells were washed three times with PBS and
289 further cultured at 37°C for 4 days in FBS-free DMEM supplemented with 0.5
290 μg/mL trypsin (Sigma Aldrich, 9002-07-7) until a clear cytopathic effect was
291 visible. The recombinant viruses were then checked by RT-PCR.

292

293 **Immunofluorescence microscopy**

294 Immunofluorescence experiments were performed using μ-Slide 8 Well Chamber
295 Slide-well (iBidi GmbH, Munich, Germany) and the following antibody dilutions:
296 anti-NSP5 guinea pig serum 1:1,000; anti-NSP2 guinea pig serum 1:200; anti-
297 VP2 guinea pig serum 1:500; anti-VP6 mouse monoclonal antibody 1:1,000;
298 Alexa Fluor 488-conjugated anti-mouse, 1:500 (Life Technologies), and TRITC-
299 conjugated anti-guinea pig, 1:500 (Life Technologies).

300

301 **5-Ethynyl-Uridine (EU) labeling**

302 Newly synthesized RNAs were labeled by including 2 mM 5-ethynyl uridine (EU)
303 into the cell culture medium, and modified incorporated nucleotides were reacted
304 with an azide-conjugated fluorophore Alexa-488 following the manufacturer's
305 protocol for Click-iT RNA Alexa Fluor 488 imaging kit (Thermo Fisher Scientific).
306 Cell nuclei were stained with ProLong™ Diamond Antifade Mountant with 4',6-
307 diamidino-2-phenylindole (DAPI, Thermo Scientific). Samples were imaged using
308 a confocal setup (Zeiss Airyscan equipped with a 63x, NA=1.3 objective), and the
309 images were processed using ZEN lite software.

310

311 **RNA Fluorescence in situ Hybridization (FISH)**

312 Rotavirus-infected MA104 cells were fixed with 4% (v/v) paraformaldehyde in
313 nuclease-free Dulbecco's phosphate saline buffer (DPBS) for 10 min at room
314 temperature. Samples were washed twice with DPBS, and then permeabilized
315 with 70% (v/v) ethanol in RNase-free water at +4°C for at least 1 hour prior to
316 hybridization. Permeabilized samples were re-hydrated for 5 min in a pre-
317 hybridization buffer (300 mM NaCl, 30 mM trisodium citrate, pH 7.0 in nuclease-
318 free water, 10 % v/v formamide, supplemented with 2 mM vanadyl ribonucleoside
319 complex). Re-hydrated samples were hybridized with 62.5 nM of an equimolar
320 mixture of Cy3-labelled DNA probes designed to target the coding region of the
321 gene segment 6 of simian rotavirus A/SA11 (Genbank Acc. AY187029.1) using
322 Stellaris Probe Designer v2 software (LCG Biosearch Technologies), in a total
323 volume of 200 µl of the hybridization buffer (Stellaris RNA FISH hybridization
324 buffer, SMF-HB1-10, Biosearch Technologies, supplemented with 10% v/v of
325 deionized formamide). After 4-8 hours of incubation at 37°C in a humidified
326 chamber, samples were briefly rinsed with the wash buffer (300 mM NaCl, 30
327 mM trisodium citrate, pH 7.0, 10 % v/v formamide in nuclease-free water), after
328 which a fresh aliquot of 300 µl of the wash buffer was applied to each sample
329 and incubated twice at 37°C for 30 min. After 2 washes, nuclei were briefly
330 stained with 300 nM DAPI solution in 300 mM NaCl, 30 mM trisodium citrate, pH
331 7.0, and the samples were finally rinsed with and stored in the same buffer
332 without DAPI prior to imaging.

333

334 **Transmission electron microscopy.** MA104 cells were seeded at 1×10^5 cells in
335 2 cm^2 wells onto sapphire discs and infected at MOI of 75 FFU/cell. At 10 hpi,
336 cells were fixed with 2.5% glutaraldehyde in 100 mM Na/K phosphate buffer, pH
337 7.4 for 1 h at 4°C and kept in that buffer overnight at 4°C. Afterward, samples
338 were postfixated with 1% osmium tetroxide in 100 mM Na/K phosphate buffer for
339 1h at 4°C and dehydrated in a graded ethanol series starting at 70%, followed by
340 two changes in acetone, and embedded in Epon. Ultrathin sections (60 to 80 nm)

341 were cut and stained with uranyl acetate and lead citrate (33). Samples were
342 analysed in a transmission electron microscope (CM12; Philips, Eindhoven, The
343 Netherlands) equipped with a charge-coupled-device (CCD) camera (Ultrascan
344 1000; Gatan, Pleasanton, CA, USA) at an acceleration of 100 kV.

345

346 **λ -Protein phosphatase and Calf Intestinal Alkaline Phosphatase Assays**

347 Cellular extracts were incubated with 2,000 units of λ -protein phosphatase (λ -
348 Ppase) (New England Biolabs) in 50 mM Tris-HCl (pH 7.5), 0.1 mM EDTA, 5 mM
349 DTT, 0.01% Brij 35, and 2 mM MnCl₂. The mixture was incubated at 30°C for 2 h.
350 Samples were loaded in SDS-PAGE and analysed by Western blotting.

351 For the Calf Intestinal Alkaline Ppase (CIP) assay, cellular extracts were
352 incubated with 1,000 units of CIP (New England Biolabs) in CutSmart™ reaction
353 buffer (New England Biolabs) and incubated at 30°C for 2h. Samples were
354 subjected to SDS-PAGE and analysed by Western blotting.

355

356 **Electrophoresis of Viral dsRNA Genomes.**

357 Cells were infected with the recombinant viruses at MOI of 5 and were lysed 16
358 hours post infection. Total RNA was extracted from lysed cells with RnaZol®
359 (Sigma-Aldrich) according the manufacturer's protocol and the dsRNA segments
360 were resolved on 10% (wt/vol) poly-acrylamide gels (PAGE) for 2 hours at 180
361 Volts and visualized by ethidium bromide staining (1 μ g/ml).

362

363 **Protein Analysis**

364 Proteins derived from rRVs-infected cellular extract were separated on an SDS-
365 PAGE for 2 hours at 35 mA and transferred to polyvinylidene difluoride
366 membranes (Millipore; IPVH00010) for 1 hour and 30 minutes at 300 mA (24).
367 For protein analysis membranes were incubated with the following primary
368 antibodies: anti-NSP5 (1:5,000) (16), anti-VP2 (1:5,000) (10), anti-NSP2 guinea
369 pig sera (1:2,000). The membranes were then incubated with the corresponding
370 horseradish peroxidase (HRP)-conjugated goat anti-guinea pig (1:10,000;

371 Jackson ImmunoResearch). Mouse HRP-conjugated anti-actin mAb (1:35,000)
372 (clone AC-15, Sigma-Aldrich) was used as loading control.
373 Signals were detected using the enhanced chemiluminescence system (Pierce
374 ECL Western blotting substrate; Thermo Scientific).

375

376 **Statistics used**

377 Statistical analysis and plotting were performed using GraphPad Prism 6
378 software (GraphPad Prism 6.0, GraphPad Software Inc., La Jolla, CA, USA).
379 Error bars represent standard deviation. Data were considered to be statistically
380 significant when $p < 0.05$ by Student's t test.

381

382 **RESULTS**

383 **Generation of gs11 mutated recombinant RVs**

384 Recombinant rotaviruses (simian rotavirus A strain SA11) carrying different
385 mutations in the NSP5 coding region of gs11 were obtained using a recently
386 developed reverse genetics protocol (29). Two essential additional modifications
387 were introduced to *trans*-complement the potential loss of NSP5 function in the
388 rRV mutants: i) an additional T7-driven plasmid encoding the ORF of wt NSP5
389 (i.e., without gs11 5' and 3' UTRs) was included in the transfection step of BHK-
390 T7 cells; and ii) each rescued rRV was amplified in a stable transfectant cell line
391 MA-NSP5, supplying the wt NSP5 in trans. Crucially, we have successfully
392 established a novel MA-NSP5 cell line to support the replication of NSP5-
393 deficient recombinant viruses to enable their further in-depth characterisation.
394 Both steps (i) and (ii) were absolutely required for rescuing the NSP5 KO virus,
395 confirming the essential role of NSP5 for RV replication. These mutants, as well
396 as additional stable cell lines generated for this study as described in Materials
397 and Methods, are summarised in Table 1.

398

399 **rRV-NSP5/KO**

400 NSP5 expression and localisation to viroplasms in virus-infected cells have been
401 considered essential for virus replication (12, 13, 25, 34). Previous studies, using

402 siRNA targeting gs11 mRNA have shown strong impairment of RV replication
403 (12, 13). In order to investigate the effects of point mutations and deletions within
404 the NSP5 gene, we took advantage of the established trans-complementing
405 MA104 cell line stably expressing NSP5. In addition, we also made two cell lines
406 expressing NSP2-mCherry and NSP5-EGFP fusions, which are rapidly and
407 efficiently recruited into viroplasms upon virus infection (Table 1) (7, 22).

408 Here we provide direct demonstration of the role of NSP5 in RV replication, using
409 an NSP5 knock out rRV (termed rRV-NSP5/KO) generated by reverse genetics.
410 To rescue the NSP5/KO strain, a stop codon at position 18Y was introduced (Fig.
411 1A-B). Analysis of MA104-virus-infected cell extracts confirmed the presence of
412 NSP2 and VP2, but not of NSP5 (Fig. 2A). Moreover, we did not detect
413 viroplasms containing NSP2, VP2 or VP6 in both MA104-infected cells and in
414 stable transfectant cell lines expressing the fluorescent fusion proteins NSP2-
415 mCherry or NSP5-EGFP (Fig. 2B). Interestingly, this indicates that the NSP5-
416 EGFP fusion protein is not able to trans-complement the lack of NSP5, and
417 indeed the rRV-NSP5/KO strain does not replicate in MA-NSP5-EGFP cells.
418 Furthermore, both genomic dsRNA synthesis and infectious progeny virus
419 production were completely abrogated in MA104 cells, but not in the trans-
420 complementing MA-NSP5 cell line (Fig. 2C). Together, these data confirm that
421 NSP5 is essential for RV replication.

422

423 **rRVs with impaired NSP5 phosphorylation**

424 To address the role of NSP5 hyperphosphorylation, we then generated a number
425 of rRVs harbouring NSP5 mutations previously known to impact NSP5
426 phosphorylation. We first generated an rRV carrying an S67A mutation (rRV-
427 NSP5/S67A) (Table 1 and Fig. 3A-B). Its replication in wild type MA104 cells was
428 strongly impaired (Fig. 3B right panel), resulting in approximately a 100-fold
429 reduction of the infectious progeny virus titre at different time points post-infection
430 (Fig. 3C). Despite the overall reduction of replication fitness, the rRV-NSP5/S67A
431 mutant virus was stable after 10 passages in the wild-type MA104 cells,
432 confirmed by the sequencing of the progeny virus. Consistent with our previous

433 results, the NSP5-S67A mutant was not hyper-phosphorylated in all cell lines
434 tested, including MA104, U2OS and Caco-2 cells (Fig. 3D), further confirming the
435 role of Ser67 in the initiation of NSP5 phosphorylation cascade (24). While the wt
436 rRV yielded multiple hyper-phosphorylated NSP5 isoforms, the NSP5/S67A
437 mutant mostly produced a single, homogeneous form of NSP5 with an apparent
438 mass of 26 kDa that could be detected in the virus-infected cell extracts at 5 or
439 10 hpi (Fig. 3E). Enzymatic de-phosphorylation with λ -Ppase and alkaline Calf
440 Intestinal Ppase (CIP), previously used to discriminate phosphorylated from non-
441 phosphorylated NSP5 (19), further corroborated the observed lack of
442 NSP5/S67A phosphorylation (Fig. 3F). Because of the differences in the
443 molecular weight markers used, the NSP5 band with the fastest PAGE mobility
444 has been traditionally described as 26 kDa, and the most abundant one as 28
445 kDa. Since this nomenclature has been used in many publications, we have
446 preferred to maintain it, despite current PAGE migrations do not correspond to
447 the markers presently used.

448 We then generated two additional rRVs harbouring truncated versions of NSP5,
449 one lacking the 18 AA long C-terminal tail (rRV-NSP5/ Δ T), and the second one
450 with a 5 AA deletion (176-YKKKY-180) just upstream of the tail region (rRV-
451 NSP5/ Δ 176-180) (Table 1 and Fig. 1A-B). Despite the presence of Ser67, and
452 the lack of Thr and Ser residues within the deletions, both mutants did not show
453 a classical hyperphosphorylation pattern (Fig. 4A) and failed to replicate,
454 confirmed by the absence of *de novo* synthesis of genomic dsRNA (Fig. 4B).

455 We also investigated viroplasm formation in cells infected with these rRV
456 mutants. At early infection (5 hpi), the rRV-NSP5/S67A mutant produced
457 structures resembling viroplasms that appeared smaller and more
458 heterogeneous in shape compared to the regular, spherical ones produced
459 during the wt rRV infection (Fig. 5A upper panel and Fig. 5B). Remarkably,
460 during late infection (10-12 hpi), the rRV-NSP5/S67A mutant produced multiple
461 NSP5-containing aberrant structures, as well as fibre-like structures that became
462 more apparent during late infection (12 hpi) (Fig. 5A lower panel and Fig. 5B).

463 Interestingly, these structures produced by rRV-NSP5/S67A were
464 morphologically similar to those observed during wt RV infection of MA104 cells
465 silenced for cellular kinase CK1 α , previously shown to be required for NSP5
466 phosphorylation (25). NSP2-mCherry and NSP5-EGFP fusion proteins were also
467 recruited to both types of these structures (Fig. 5C), suggesting that the observed
468 lack of phosphorylation does not affect NSP2/NSP5 interactions. Furthermore,
469 the NSP5/S67A mutant and additional viroplasmic proteins NSP2, VP6 and VP2
470 (Fig. 5D) were all present in the aberrant structures, suggesting that they could
471 also represent sites of virus replication.

472 In contrast, no viroplasms containing NSP5, NSP2 or VP2 were observed when
473 MA104 cells were infected with the rRV-NSP5/ Δ T and rRV-NSP5/ Δ 176-180
474 deletion mutants. Interestingly, these mutants yielded fibre-like structures
475 containing only VP6 protein (Fig. 5E-F). Similar VP6-fibres are normally formed
476 when VP6 is over-expressed in cells in the absence of other viral proteins (35,
477 36).

478 Taken together, these results confirm the role of NSP5 hyper-phosphorylation for
479 controlling the assembly of regular-shaped viroplasms, highlighting the key role
480 of the C-terminal tail in the formation of RV viral factories.

481

482 **RNA accumulation in aberrant structures**

483 Having examined the viral protein composition of the aberrant viroplasms formed
484 during infection with rRVs exhibiting impaired NSP5 phosphorylation, we then
485 assessed their RNA content. Viral RNA transcripts were labelled by incorporation
486 of 5-ethynyl uridine (5-EU) in actinomycin D-treated RV-infected cells, and total
487 viral ssRNA was visualized by reacting with Alexa-488-azide, as described in
488 Materials and Methods. As expected, most viral transcripts localised in
489 viroplasms of rRV-wt infected cells (Fig. 6A), consistent with the roles of
490 viroplasms in supporting the viral replication and assembly. In contrast, no viral
491 RNA transcripts could be detected in the aberrant structures in both wt MA104 or
492 MA-NSP2-mCherry cells infected with the rRV-NSP5/S67A mutant (Fig. 6A).

493 RNA accumulation in viroplasms was instead restored when infecting MA-NSP5
494 cells that supply wild type NSP5 in *trans* (Fig. 6A-lower panel).

495 Although we did not detect RNA in aberrant structures (or viroplasms) in rRV
496 NSP5/S67A-infected MA104 cells using 5-EU staining, this mutant could still
497 replicate (Fig. 3C). We then explored whether rRV-NSP5/S67A transcripts could
498 accumulate in viroplasms, albeit with much lower efficiency, i.e., beyond the
499 sensitivity limit of 5-EU staining. For this purpose, we used single molecule RNA
500 fluorescence in situ hybridisation (smFISH) to identify the sites of RV
501 transcription. At 10 hpi, abundant gs6 transcripts could be detected in all
502 viroplasms identified in MA-NSP5-EGFP cells infected with the rRV-wt (Fig. 6B).
503 Conversely, the rRV-NSP5/S67A-infected cells had sparse EGFP-tagged
504 structures, but less than 20% of them contain gs6 RNA (Fig. 6B-C). Interestingly,
505 the less frequently occurring rod-like aberrant structures also showed gs6 RNA
506 accumulation, further suggesting that these structures could represent
507 replication-functional organelles.

508 In contrast, smFISH performed on cells infected with the rRV-NSP5/ Δ T showed
509 diffuse distribution of gs6 RNA that did not localise to any structures resembling
510 viroplasms (Fig. 6B), also failing to support the virus genome replication (Fig.
511 4B).

512 We then examined the ultrastructures of viroplasms with altered morphologies in
513 the RV mutant rRV-NSP5/S67A using electron microscopy. Upon infection with
514 rRV-wt (Fig. 7A, left panel), multiple membrane-less electron dense inclusions
515 encircled by the well-defined endoplasmatic reticulum (ER) filled with triple-
516 layered particles were present in cells. At late infection points (10 hpi), filled with
517 triple-layered particles (TLPs) ER appeared to adopt a more tubular morphology,
518 suggesting a successive step in the virus egress. In contrast, the rRV-
519 NSP5/S67A-infected cells contained only few immature viroplasms that lacked
520 the ER network filled with TLPs (Fig. 7A, right panel). Only few immature
521 particles containing transient lipid membranes could be identified in cells infected
522 with rRV-NSP5/S67A mutant (Fig. 7A, left panel). Furthermore, the observed
523 immature viroplasms also appeared to be less-electron dense, likely due to their

524 lower RNA composition and, subsequently, decreased number of available
525 phosphate groups that bind UO^{2+} ions during the EM staining procedure.
526 Together, these data strongly support the role of NSP5 phosphorylation in
527 maintaining the viral RNA production and genome replication in viroplasms.

528

529 **The mechanism of NSP5 hyper-phosphorylation**

530 We have previously proposed a model of the hierarchical NSP5
531 hyperphosphorylation associated with the assembly of viroplasms that involves a
532 three-step mechanism: i) initial interaction of non-phosphorylated NSP5 with
533 NSP2 (or VP2); ii) phosphorylation of Ser67 by $CK1\alpha$. This step does not take
534 place when NSP5 is expressed alone; iii) hyper-phosphorylation of NSP5
535 triggered by Ser67 phosphorylation that requires the 18 AA long C-terminal tail
536 (24).

537 Here, we have investigated the phosphorylation mechanism of NSP5 during RV
538 infection using a number of NSP5 phosphorylation-negative rRV strains and
539 MA104-derived stable transfectant cell lines (Table 1). We demonstrated that
540 despite the presence of Ser67, deletion mutant NSP5/ ΔT was not phosphorylated
541 and failed to form viroplasms. We have previously shown that co-expression of
542 NSP5/ ΔT was also unable to trigger the phosphorylation cascade of NSP5/S67A,
543 while other NSP5 mutants referred hereafter as activators of phosphorylation,
544 e.g., NSP5/ $\Delta 3$ did (24). Interestingly, upon co-infection with two rRVs
545 NSP5/S67A and NSP5/ ΔT , both mutated NSP5 variants were not phosphorylated
546 (Fig. 8A) (8, 19, 24, 26). This result was supported further by infecting the MA104
547 transfectant cell line stably expressing NSP5- ΔT (MA- ΔT) with the rRV-
548 NSP5/S67A strain (Table 1 and Fig. 8B, lanes 3-4). The NSP5- $\Delta 176-180$ mutant
549 was also unable to induce phosphorylation of NSP5/S67A following the co-
550 infection with the two rRVs, despite both containing Ser67 and the C-terminal tail.
551 This result suggests that the 'activator' NSP5 needs to be also hyper-
552 phosphorylated (Fig. 8C).

553 In MA- Δ T cells infected with rRV-NSP5/S67A mutant strain aberrant viroplasms
554 were produced (Fig. 8E), similar to those seen in wt MA104 cells, which did not
555 support virus replication compared to the wt virus (Fig. 8F).

556 In contrast to NSP5/ Δ T, the NSP5 deletion mutant lacking amino acids 80-130,
557 (NSP5/ Δ 3) becomes hyper-phosphorylated when expressed alone and can
558 function as an activator of the NSP5/S67A phosphorylation (19, 24). We
559 therefore asked whether an MA104 stable cell line expressing the deletion
560 mutant NSP5/ Δ 3 (MA- Δ 3) and infected with the rRV-NSP5/S67A strain was able
561 to trigger hyperphosphorylation of NSP5/S67A and as a consequence, sustain
562 replication of the mutant rRV strain. As shown in Fig. 8B (lanes 5-6) NSP5/S67A
563 was hyper-phosphorylated in presence of NSP5/ Δ 3 mutant and confirmed by the
564 λ Ppase treatment (Fig. 8D), although it did not completely rescue the
565 phosphorylation pattern of NSP5 normally observed in rRV-wt infection. When
566 loading large amounts of NSP5/S67A, we have occasionally observed a second
567 faint band with reduced mobility, as in Fig. 8B, lane 2 (indicated with *).
568 Interestingly, regular round-shaped structures resembling viroplasms, containing
569 NSP5, NSP2 and VP2 with peripheral localisation of VP6, were recovered in
570 these cells infected with rRV-NSP5/S67A, and yet viral replication was
571 nevertheless impaired (Fig. 8E-F). Consistently, the electron microscopy images
572 showed structures of aberrant viroplasms similar to those obtained in MA104 wt
573 cells (Fig. 7B, right panel).

574 The NSP5 phosphorylation negative mutants of the two other rRVs (NSP5/ Δ T
575 and NSP5/ Δ 176-180), did not undergo hyper-phosphorylation in MA- Δ T or MA- Δ 3
576 cell lines (Figs. 9A-B). In both cases, viroplasms formation and virus replication
577 were not rescued (Figs. 9C-D and 9E-F). Interestingly, apparently normal round-
578 shaped structures were observed in MA- Δ 3 cells, which, however, recruited
579 significantly less VP6 (Fig. 9C-D). In addition, the previously observed VP6 spiky
580 structures were not detected in these cells (Figs. 9C-D). Similar results were
581 obtained with the rRV-NSP5/KO virus strain, which in MA- Δ 3 cells did not
582 replicate and also showed spherical structures that contained NSP5 and NSP2,
583 but not VP6 (Fig. 10A-C).

584 Taken together, our data support a model of NSP5 hyper-phosphorylation, which
585 absolutely requires the presence of the C-terminal tail, and the AA residues 176-
586 180. Furthermore, NSP5 hyperphosphorylation requires Ser67 phosphorylation
587 to initiate the phosphorylation cascade, thus playing a key role in the assembly of
588 replication-competent viral factories.

589

590 **DISCUSSION**

591 Rotaviruses replicate within cytoplasmic viral factories, or viroplasms. Most RV
592 assembly intermediates, i.e., single layered particles (cores) and double-layered
593 particles (DLPs) are primarily concentrated in viroplasms. Following budding of
594 DLPs into the lumen of the endoplasmic reticulum, the immature particles
595 acquire a transient envelope, as well as the outer capsid proteins VP4 and VP7,
596 resulting in a mature triple-layered virion. Moreover, downregulation of
597 expression of the most abundant viroplasm-forming proteins NSP5 and NSP2
598 severely impacts on the formation of viroplasms and production of virus progeny
599 (13, 15, 25, 34). In light of these observations, viroplasms have long been
600 recognised as essential compartments supporting the RV replication.

601 Of the two non-structural proteins involved in viroplasm assembly, NSP5 appears
602 to play a crucial role by potentially providing a scaffold that allows for recruitment
603 of additional viral proteins. Only when NSP5 is co-expressed with NSP2 and/or
604 VP2, these proteins assemble into the viroplasm-like structures (VLS), which are
605 also capable to recruit additional structural proteins including VP1, VP2 and VP6
606 (8, 10). Given these observations, we hypothesised that complete removal of
607 NSP5 would be lethal for RV replication. Using a modified reverse genetics
608 system for rotaviruses (29), here we provide the first direct evidence of the
609 essential role of NSP5 in viroplasm formation and viral replication. In order to
610 characterise replication-deficient NSP5-negative mutants, we have established a
611 trans-complementing system that provides NSP5 to the virus both transiently in
612 BHK-T7 cells, and stably in NSP5-producing MA104 cell line (MA-NSP5), thus
613 enabling facile isolation of rRVs lacking functional NSP5. Using this approach,
614 we have demonstrated that NSP5-deficient rRV was unable to form viroplasms

615 and replicate in the wt MA104 cells, while the viroplasm formation and viral
616 replication were efficiently rescued in the trans-complementing MA-NSP5 cell
617 line. Interestingly, the rRVs generated using this method also failed to
618 incorporate dsRNA originating from the NSP5-encoding mRNA lacking the 5' and
619 3' untranslated regions (UTRs), further suggesting the essential roles of UTRs for
620 genome packaging in RVs (37, 38).

621 NSP5 hyper-phosphorylation has been previously implicated in the regulation of
622 NSP5 assembly into viroplasms. This phosphorylation, however, requires the
623 interaction of NSP5 with, either NSP2 or VP2, as NSP5 is not phosphorylated
624 when expressed alone (8, 22, 23). Previous studies suggest that activation of
625 NSP5 hyper-phosphorylation may require a conformational change that leads to
626 its efficient hyper-phosphorylation via a positive feedback loop mechanism (8, 23,
627 24). Two regions comprising the N-terminal amino acids 1-33 (region 1) and the
628 central region amino acids 81-130 (region 3) have been reported to prevent
629 NSP5 phosphorylation in the absence of other viral proteins, while the 18 amino
630 acids long C-terminal tail was found to be essential for its phosphorylation (8, 23,
631 24).

632 Here, we have shown that all three rRV mutants S67A, Δ T and Δ 176-180
633 expressing the phosphorylation-negative NSP5 variants were unable to form
634 round-shaped viroplasms upon infection of MA104 cells. Interestingly, further
635 analysis of these mutants reveals some key differences between each NSP5
636 variant. While rRV-NSP5/S67A strain formed aberrant structures resembling
637 viroplasms that poorly support RV replication, this variant was still capable of
638 producing the infectious progeny, in contrast to the two other rRV mutant strains.
639 Interestingly, the phenotype observed with the NSP5 mutant S67A was
640 essentially the same as the one previously reported with the wt virus infecting
641 MA104 cells silenced for expression of CK1 α , which is involved in
642 phosphorylating Ser67 and initiating the hyper-phosphorylation cascade (24, 25).
643 It has recently been shown that CK1 α is also involved in phosphorylating NSP2,
644 controlling the formation of rotavirus viral factories (39). Our data obtained with
645 the rRV-NSP5/S67A mutant strongly suggest that the lack of NSP5 hyper-

646 phosphorylation determines both the morphogenesis of viroplasms and their
647 capacity to support RV genome replication. We cannot rule out the role of NSP2
648 phosphorylation in assembly of viroplasms since NSP2 is also likely to be
649 phosphorylated by CK1 α upon infection of the rRV-NSP5/S67A strain. Despite
650 the formation of aberrant structures resembling viroplasms, the amount of RNA
651 produced within those structures in rRV-NSP5/S67A-infected MA104 cells was
652 practically below the detection limit of the 5-EU labelling, while the RNA
653 replication was fully rescued in the trans-complementing MA-NSP5 cell line (Fig.
654 5). It is unlikely that the viral mRNAs produced in MA104 wt cells infected with
655 the rRV-NSP5/S67A strain was degraded faster, as most of the ssRNA
656 synthesised is a consequence of the secondary round of transcription from the
657 newly made dsRNA-containing particles. Indeed, very low amounts of dsRNA
658 were detected during the infection of MA104 cells. smFISH results confirmed the
659 presence of small amounts of RV (+)ssRNA in some of these aberrant structures.
660 This result is consistent with the finding that the rRV-NSP5/S67A strain did
661 replicate, albeit at much lower levels than the rRV-wt. Thus, these structures are
662 likely to sustain virus replication with decreased efficiency, which was further
663 confirmed by the electron microscopy analysis of MA104 cells infected with the
664 rRV-NSP5/S67A strain.

665 The important role of NSP5 hyper-phosphorylation was further supported by the
666 results obtained with the two phosphorylation-negative mutant strains NSP5/ Δ T
667 and NSP5/ Δ 176-180 that possess Ser67 and yet failed to form viroplasms in
668 MA104 cells. Surprisingly, the Δ 176-180 mutant, containing the C-terminal tail
669 has also failed to form viroplasms in MA104 cells, despite the absence of Ser or
670 Thr within the chosen 176-180 region. Both phosphorylation-negative mutants
671 tested did not replicate in MA104 cells and we could not detect any structures
672 containing viral RNA.

673 Using the NSP5 mutant strains described above and the established stable
674 transfectant MA104 cells we were able to investigate the molecular mechanism
675 that leads to NSP5 hyperphosphorylation. We showed that the NSP5/S67A
676 mutant from the rRV was indeed hyperphosphorylated, albeit not completely,

677 when infecting MA- Δ 3 cells, restoring the round-shape morphology of the
678 structures resembling viroplasms with a complete absence of the aberrant
679 structures observed in MA104 cells. This finding strongly suggests that
680 impairment of NSP5 phosphorylation is the direct cause of the formation of the
681 aberrant structures in the cytosol of the infected cell. Despite the fact that these
682 structures appeared morphologically similar to the classical round-shaped
683 viroplasms in MA- Δ 3 cells, the presence of VP6 around these structures was only
684 observed with the hyperphosphorylated NSP5/S67A mutant, in contrast to the
685 other NSP5 phosphorylation-negative mutants. One possibility is that, during RV
686 infection, accumulation of VP6 in round-shaped viroplasms requires a full-length
687 hyperphosphorylated NSP5, as well as phosphorylation of multiple serine
688 residues likely by CK2 (17, 26). Moreover, the round-shaped structures found in
689 MA- Δ 3 cells infected with rRV-NSP5/KO failed to contain VP6.

690 The observed failure to rescue the replication of the rRV-NSP5/S67A strain to the
691 wt levels in MA- Δ 3 cells could be the consequence of the incomplete recovery of
692 the complex pattern of phosphorylated isoforms of wt NSP5. This suggests that
693 some intermediate isoforms might be important for the formation of fully
694 functional replication-competent viroplasms.

695 We propose a model of the complex hierarchical mechanism of NSP5 hyper-
696 phosphorylation during RV infection (Fig. 11). It involves (a) interaction of NSP5
697 with either NSP2 or VP2, required to (b) make Ser67 available for CK1 α
698 phosphorylation. This initial step is then sequentially completed (c) by CK2-
699 mediated phosphorylation of other serines to generate the NSP5 'activator',
700 during a step dependent (d) on the interaction of the Ser67-phosphorylated
701 molecules with the non-phosphorylated partners in the NSP5 oligomeric
702 complexes. Alternatively (c'), oligomers could be formed before the activation
703 step. NSP5 interactions mediated by the carboxy-terminal tails T result in (e)
704 substrate activation and a fully hyperphosphorylated NSP5. This process leads to
705 (f) the assembly of viroplasms scaffolds containing NSP2, and (g) recruitment of
706 VP6, as well as the other viroplasmic proteins, VP1, VP2, VP3 to assemble
707 replication-competent viroplasms.

708 The hierarchical phosphorylation of proteins appears to be a common
709 mechanism regulating many cellular processes. In mammalian cells, hierarchical
710 phosphorylation has been described for β -catenin, in which Ser 45
711 phosphorylated by CK1 α primes it for hyperphosphorylation by glycogen
712 synthase kinase-3 (GSK-3) (40, 41), which triggers its ubiquitination and
713 proteasomal degradation (42). A similar phosphorylation mechanism has recently
714 been described for a non-structural protein NS5A of the Hepatitis C Virus (HCV),
715 with the hyper-phosphorylation cascade primed by the initial phosphorylation of
716 Serine 225 by CK1 α , and the subsequent phosphorylation of neighbouring
717 residues involving other kinases (43, 44). Moreover, the NS5A phosphorylation
718 was shown to play a key role in controlling the establishment of replication
719 complexes during HCV infection (45). Similarly, a number of other non-structural
720 viral proteins have been shown to undergo multiple phosphorylation events
721 during virus infection, suggesting that this complex post-translational
722 modifications play a pivotal role in orchestrating the assembly of replication-
723 competent viral factories (46–48).

724

725

726 **ACKNOWLEDGEMENTS**

727 We thank John T. Patton, Asha Ann Philipp and Jin Dai (Indiana University,
728 Bloomington, USA), Yuta Kanai and Takeshi Kobayashi (Osaka University,
729 Osaka) and Albie Van Dijk (North-West University, South Africa) for helpful
730 discussions on the establishment of the reverse genetics system. We are grateful
731 to Naoto Ito for providing BHK-T7 cells.

732

733

734

735

736

737

738

739

740

741

742

743 **FIGURE LEGENDS**

744

745 **Figure 1.** A) Schematic representation of mutations in gs11 of the corresponding
746 rRV strains. Sequences mutated or deleted in NSP5 are indicated. B), Profiles of
747 viral dsRNAs of the different rRV strains generated grown in MA-NSP5 cells.
748 gs11, indicated in red with *.

749

750 **Figure 2. Characterisation of rRV-NSP5/KO.** A) Western blot of MA104 cells
751 extracts infected with rRV-wt and rRV-NSP5/KO strains (MOI of 1 FFU/cell). B)
752 Confocal immunofluorescence microscopy of MA104, MA-NSP2-mCherry and
753 MA-NSP5-EGFP cells infected with rRV-wt or rRV-NSP5/KO (MOI of 1 FFU/cell),
754 using antibodies for NSP5, NSP2, VP2 and VP6, as indicated. Scale bar, 15 μ m.
755 C) Electrophoretic migration pattern of dsRNAs extracted from rRV-NSP5/KO
756 strain grown in MA-NSP5 or MA104 cells. Genome segments 1-11 are indicated
757 to the left.

758

759 **Figure 3. Characterisation of rRV-NSP5/S67A.** A) Schematic representation of
760 rRV-NSP5/S67A gs11 and sequence of NSP5 wt and S67A mutant (highlighted).
761 B) Electrophoretic pattern of dsRNA genome segments of rRV-wt and rRV-
762 NSP5/S67A strains grown in MA-NSP5 cells (left panel) and in MA104 wt cells
763 (right panel). C) Replication kinetics of rRV-wt and rRV-NSP5/S67A in MA104
764 cells. Data are expressed as the means +/- standard deviations (n=3); ***, $p <$
765 0.001 (Student's t test). D) Western blot of extracts of U2OS, Caco-2 and MA104
766 cells infected with rRV-wt or rRV-NSP5/S67A strains. E) Western blot of NSP5
767 phosphorylation pattern in MA104 cells infected with rRV-wt or rRV-NSP5/S67A
768 (MOI of 1 FFU/cell) at 5 and 10 hpi. F) Western blot of λ -Ppase and alkaline

769 Ppase treatment of lysates of MA104 cells infected with rRV-wt or rRV-
770 NSP5/S67A. Protein bands corresponding to NSP5 are shown.

771

772 **Figure 4. Characterisation of rRV-NSP5/ Δ T and rRV-NSP5/ Δ 176-180.** A)

773 Western blot of NSP5 and NSP5 mutants from MA104 cells infected with rRV-wt,

774 rRV-NSP5/ Δ T or rRV- NSP5/ Δ 176-180 at 5 hpi. B) Electrophoretic dsRNA

775 migration pattern of rRV-NSP5/ Δ T and rRV-NSP5/ Δ 176-180 grown in MA-NSP5

776 and MA104 cells.

777

778 **Figure 5. Viroplasms morphology in MA104 cells infected with rRV-NSP5 wt**

779 **and mutants.** Representative confocal immunofluorescence micrographs of

780 MA104 cells infected with rRV-wt and rRV-NSP5/S67A (MOI of 15 FFU/cell) at 5

781 hpi (upper panels) or 10 hpi (lower panels). Cells were stained with anti-NSP5

782 and DAPI. B) Quantitative analysis of viroplasms size (μm^2) of MA104 cells

783 infected with rRV-wt and rRV-NSP5/S67A at 5 hpi and 10 hpi. ***, $p < 0.001$; **, p

784 < 0.01 . C) Confocal immunofluorescence micrographs of MA-NSP5-EGFP and

785 MA-NSP2-mCherry cells infected with rRV-NSP5/S67A (MOI of 15 FFU/cell). D)

786 Confocal immunofluorescence micrographs of rRV-wt and rRV-NSP5/S67A

787 infected MA104 cells (MOI 15 FFU/cell) and stained at 10 hpi with the indicated

788 antibodies. E), F), Confocal immunofluorescence of MA104 cells infected with

789 rRV-NSP5/ Δ 176-180 (E) or rRV-NSP5/ Δ T (F) and stained with the indicated

790 antibodies and DAPI. Scale bar, 15 μm .

791

792 **Figure 6. Viral RNA detection in rRV NSP5/S67A infected cells.** A)

793 Representative confocal immunofluorescence micrographs of MA104 (upper

794 panel), MA-NSP5 (middle panel) and MA-NSP2-mCherry cells (lower panel)

795 infected with rRV-wt or rRV-NSP5/S67A strains and stained with anti-NSP5 (red,

796 in MA104 and MA-NSP5 cells) and EU (green). B) Single molecule RNA

797 Fluorescence In Situ Hybridisation (smFISH) on MA-NSP5-EGFP cells infected

798 with rRV-wt, rRV-NSP5/S67A or rRV-NSP5/ Δ T strains. Viroplasms detected with

799 NSP5-EGFP (green) and viral RNA (probe specific for gs6 was Cy3-conjugated,

800 red). Colocalising viroplasms and RNAs are indicated by white arrows. Scale bar,
801 15 μ m. C) Quantitative analysis of NSP5-EGFP positive structures (viroplasms)
802 for RNA (gs6) in MA-NSP5-EGFP cells infected with rRV-wt or rRV-NSP5/S67A.
803 ***, $p < 0.001$

804

805 **Figure 7. Electron microscopy of cells infected with rRV-NSP5/S67A.** High-
806 definition electron micrographs of MA104 (A) and MA- Δ 3 (B) cells infected with
807 rRV-wt (left panel) and rRV-NSP5/S67A (right panel) (MOI, 75 FFU/cell). At 10
808 hpi, cells were fixed with glutaraldehyde and processed for transmission electron
809 microscopy. V, viroplasm; m, mitochondria; mt, microtubule-bundles; Nu, nucleus.
810 The white open box indicates the immediate right magnified image. White arrows
811 indicate the endoplasmatic reticulum surrounding viroplasms; black arrowheads
812 indicate viral particles with an envelope. Scale bar, 500 nm.

813

814 **Figure 8. Phosphorylation of NSP5/S67A.** A) Western blot of extracts of
815 MA104 cells infected with rRV-NSP5/S67A or co-infected with rRV-NSP5/S67A
816 and rRV-NSP5/ Δ T. Blue arrowhead indicates NSP5/S67A. The faster migrating
817 band corresponds to NSP5- Δ T. B) Western blot of MA104, MA- Δ T and MA- Δ 3
818 cells infected with rRV-NSP5/S67A. Blue arrowhead indicates NSP5/S67A. C)
819 Western blot of extracts of MA104 cells co-infected with rRV-NSP5/S67A and
820 rRV-NSP5/ Δ 176-180. Blue arrowhead indicates NSP5/S67A. D) λ -Ppase
821 treatment of extracts of MA- Δ 3 cells infected with the rRV-NSP5/S67A strain.
822 Filled and open arrowheads indicate de-phosphorylated NSP5-S67A and NSP5-
823 Δ 3, respectively. E) Representative confocal immunofluorescence micrographs of
824 MA104, MA- Δ T and MA- Δ 3 cells infected with rRV-NSP5/S67A. Cells were
825 stained with the indicated antibodies. Scale bar, 15 μ m. F) Yield of infectious
826 virus of rRV-NSP5/S67A grown in MA-NSP5, MA104, MA- Δ T and MA- Δ 3 cells at
827 24 hpi. *, $p < 0.05$; **, $p < 0.01$.

828

829 **Figure 9. Phosphorylation of NSP5- Δ T and NSP5/ Δ 176-180 and viroplasm**
830 **formation.** Western blots (A, B) and confocal immunofluorescence micrographs

831 (C, D) of MA104, MA- Δ T and MA- Δ 3 cells infected with rRV-NSP5/ Δ T (A, C) or
832 with rRV-NSP5/ Δ 176-180 (B, D). Blue arrowhead indicates NSP5/ Δ T and
833 NSP5/ Δ 176-180, respectively. Open arrowheads indicate NSP5- Δ 3 and NSP5-
834 Δ T. Cells were stained with the indicated antibodies and DAPI. Scale bar, 15 μ m.
835 E) Single step growth of rRV-NSP5/ Δ T (left) and rRV-NSP5/ Δ 176-180 (right) in
836 MA-NSP5, MA104, MA- Δ T and MA- Δ 3 cells, as indicated. The experiment was
837 terminated at 24 hpi. **, $p < 0.01$; #, Viral titer < 300 FFU/ml.

838

839 **Figure 10. rRV NSP5/KO in infected cells.** Western blot (A) and confocal
840 immunofluorescence (B) of MA104, MA- Δ T and MA- Δ 3 cells infected with the
841 rRV-NSP5/KO strain. Cells were stained with the indicated antibodies and DAPI.
842 Scale bar, 15 μ m. C) Single step growth of rRV-NSP5/KO in MA-NSP5, MA104,
843 MA- Δ T and MA- Δ 3 cells, as indicated. The experiment was terminated at 24 hpi.
844 **, $p < 0.01$; #, Viral titer < 300 FFU/ml.

845

846 **Figure 11. Model of NSP5 hyperphosphorylation and assembly of**
847 **replication-competent viroplasms.** (a) Interaction of non-phosphorylated NSP5
848 with either NSP2 or VP2 is required to (b) induce conformational changes that
849 make S67 available for CK1 α phosphorylation (P). This initial step of the cascade
850 is then (c) sequentially completed by phosphorylation by CK2 of other residues
851 including serines in domain 4, to generate the NSP5 activator or, (c') a step of
852 interaction with non-phosphorylated molecule precedes the involvement of CK2.
853 (d) NSP5 interactions to form dimers/multimers are mediated by the carboxy-
854 terminal tails (T). (e) The primed (S67-phosphorylated) activator molecules result
855 in substrate activation and fully hyper-phosphorylated NSP5. (f) Assembly of
856 viroplasms scaffolds containing NSP2 serve to (g) recruit the other viroplasmic
857 components, VP1, VP2, VP3 and VP6 to assemble replication-competent
858 viroplasms. P; phosphorylated amino acid. *This image was created using
859 BioRender.com.

860

861 **Table 1.** Schematic representation of NSP5 and NSP2 mutants or fusion proteins

862 used to generate rRV and/or stable MA104 transfectant cell lines, used in this
863 study.

864 **REFERENCES**

- 865 1. Tate JE, Burton AH, Boschi-Pinto C, Parashar UD, World Health
866 Organization–Coordinated Global Rotavirus Surveillance Network. 2016.
867 Global, Regional, and National Estimates of Rotavirus Mortality in Children
868 <5 Years of Age, 2000–2013. *Clin Infect Dis* 62:S96–S105.
- 869 2. Parashar UD, Hummelman EG, Bresee JS, Miller MA, Glass RI. 2003.
870 Global illness and deaths caused by rotavirus disease in children. *Emerg*
871 *Infect Dis* 9:565–572.
- 872 3. Patton JT, Silvestri LS, Tortorici MA, Vasquez-Del Carpio R, Taraporewala
873 ZF. 2006. Rotavirus genome replication and morphogenesis: role of the
874 viroplasm. *Curr Top Microbiol Immunol* 309:169–87.
- 875 4. Desselberger U. 2014. Rotaviruses. *Virus Res* 190:75–96.
- 876 5. Estes MK, Greenberg HB. 2013. Rotaviruses, p. 1347–1401. *In* Health,
877 WK, Lippincott Williams Wilkins (eds.), *Fields Virology*, 6th ed. Philadelphia,
878 PA.
- 879 6. Clapp LL, Patton JT. 1991. Rotavirus morphogenesis: domains in the
880 major inner capsid protein essential for binding to single-shelled particles
881 and for trimerization. *Virology* 180:697–708.
- 882 7. Eichwald C, Rodriguez JF, Burrone OR. 2004. Characterization of rotavirus
883 NSP2/NSP5 interactions and the dynamics of viroplasm formation. *J Gen*
884 *Virol* 85:625–634.
- 885 8. Fabbretti E, Afrikanova I, Vascotto F, Burrone OR. 1999. Two non-
886 structural rotavirus proteins, NSP2 and NSP5, form viroplasm-like
887 structures in vivo. *J Gen Virol* 80:333–339.

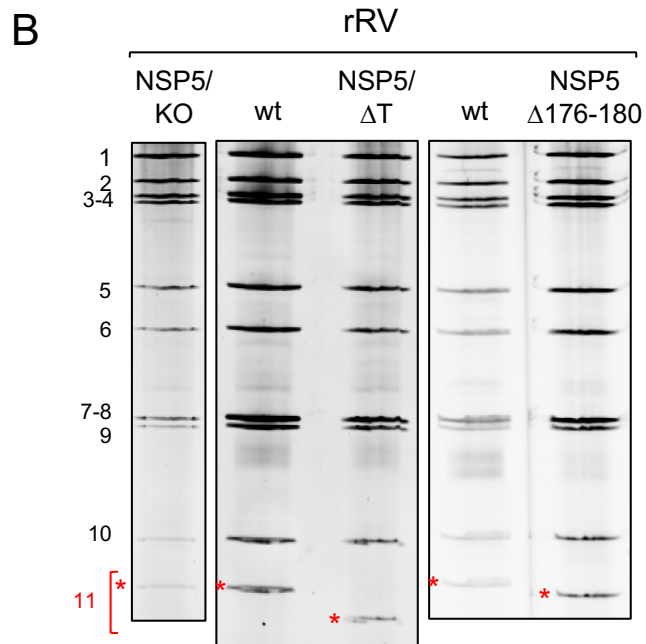
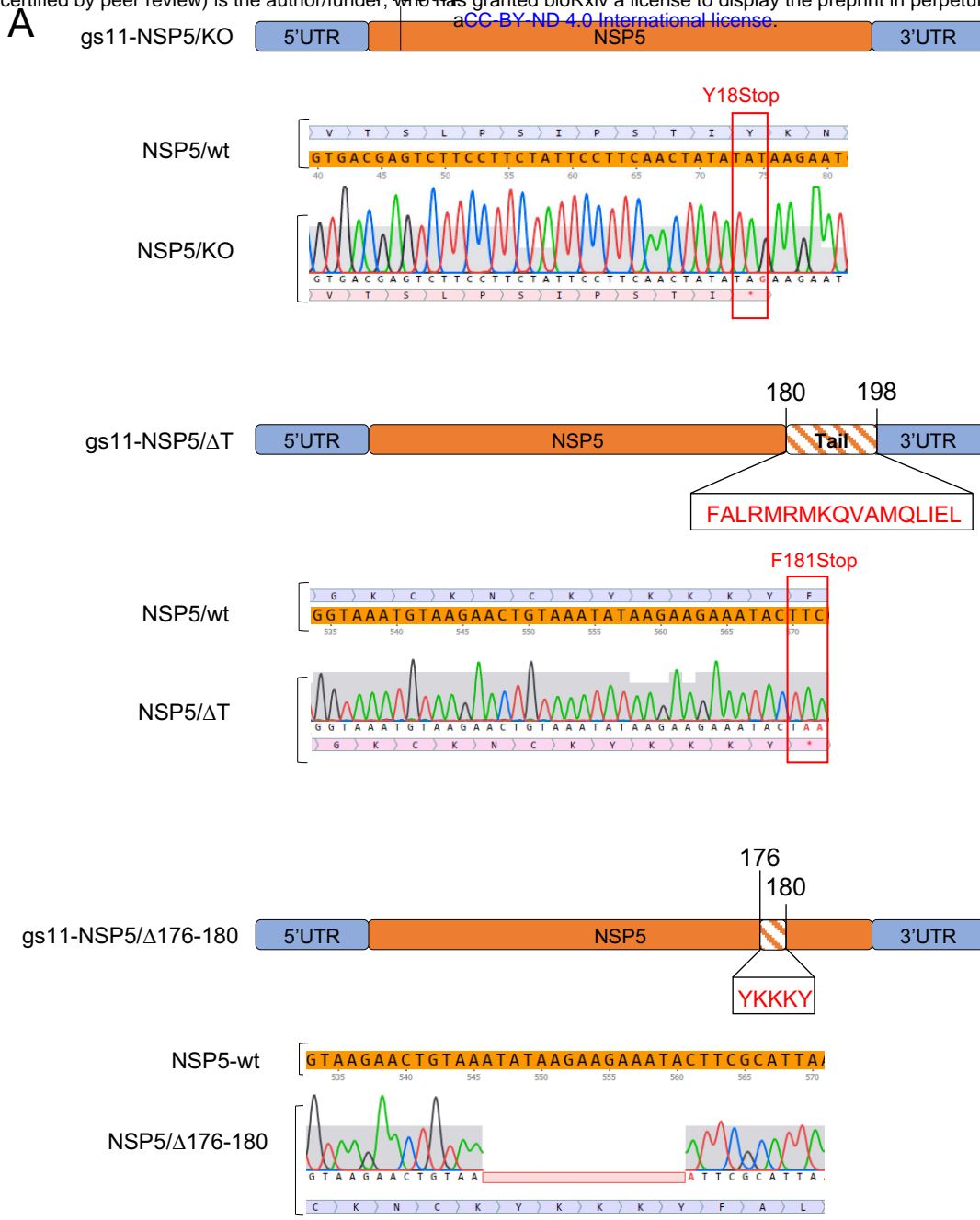
- 888 9. Poncet D, Lindenbaum P, L'Haridon R, Cohen J. 1997. In vivo and in vitro
889 phosphorylation of rotavirus NSP5 correlates with its localization in
890 viroplasms. *J Virol* 71:34–41.
- 891 10. Arnoldi F, Campagna M, Eichwald C, Desselberger U, Burrone OR. 2007.
892 Interaction of Rotavirus Polymerase VP1 with Nonstructural Protein NSP5
893 Is Stronger than That with NSP2. *J Virol* 81:2128–2137.
- 894 11. Gallegos CO, Patton JT. 1989. Characterization of rotavirus replication
895 intermediates: a model for the assembly of single-shelled particles.
896 *Virology* 172:616–27.
- 897 12. Campagna M, Eichwald C, Vascotto F, Burrone OR. 2005. RNA
898 interference of rotavirus segment 11 mRNA reveals the essential role of
899 NSP5 in the virus replicative cycle. *J Gen Virol* 86:1481–1487.
- 900 13. Lopez T, Rojas M, Ayala-Breton C, Lopez S, Arias CF. 2005. Reduced
901 expression of the rotavirus NSP5 gene has a pleiotropic effect on virus
902 replication. *J Gen Virol* 6:1609–1617.
- 903 14. Silvestri LS, Taraporewala ZF, Patton JT. 2004. Rotavirus replication: plus-
904 sense templates for double-stranded RNA synthesis are made in
905 viroplasms. *J Virol* 78:7763–74.
- 906 15. Vascotto F, Visintin M, Cattaneo A, Burrone OR. 2005. Design and
907 selection of an intrabody library produced de-novo for the non-structural
908 protein NSP5 of rotavirus. *J Immunol Methods* 301:31–40.
- 909 16. Gonzalez SA, Burrone OR. 1991. Rotavirus NS26 is modified by addition
910 of single O-linked residues of N-acetylglucosamine. *Virology* 182:8–16.
- 911 17. Sotelo PH, Schumann M, Krause E, Chnaiderman J. 2010. Analysis of
912 rotavirus non-structural protein NSP5 by mass spectrometry reveals a
913 complex phosphorylation pattern. *Virus Res* 149:104–108.

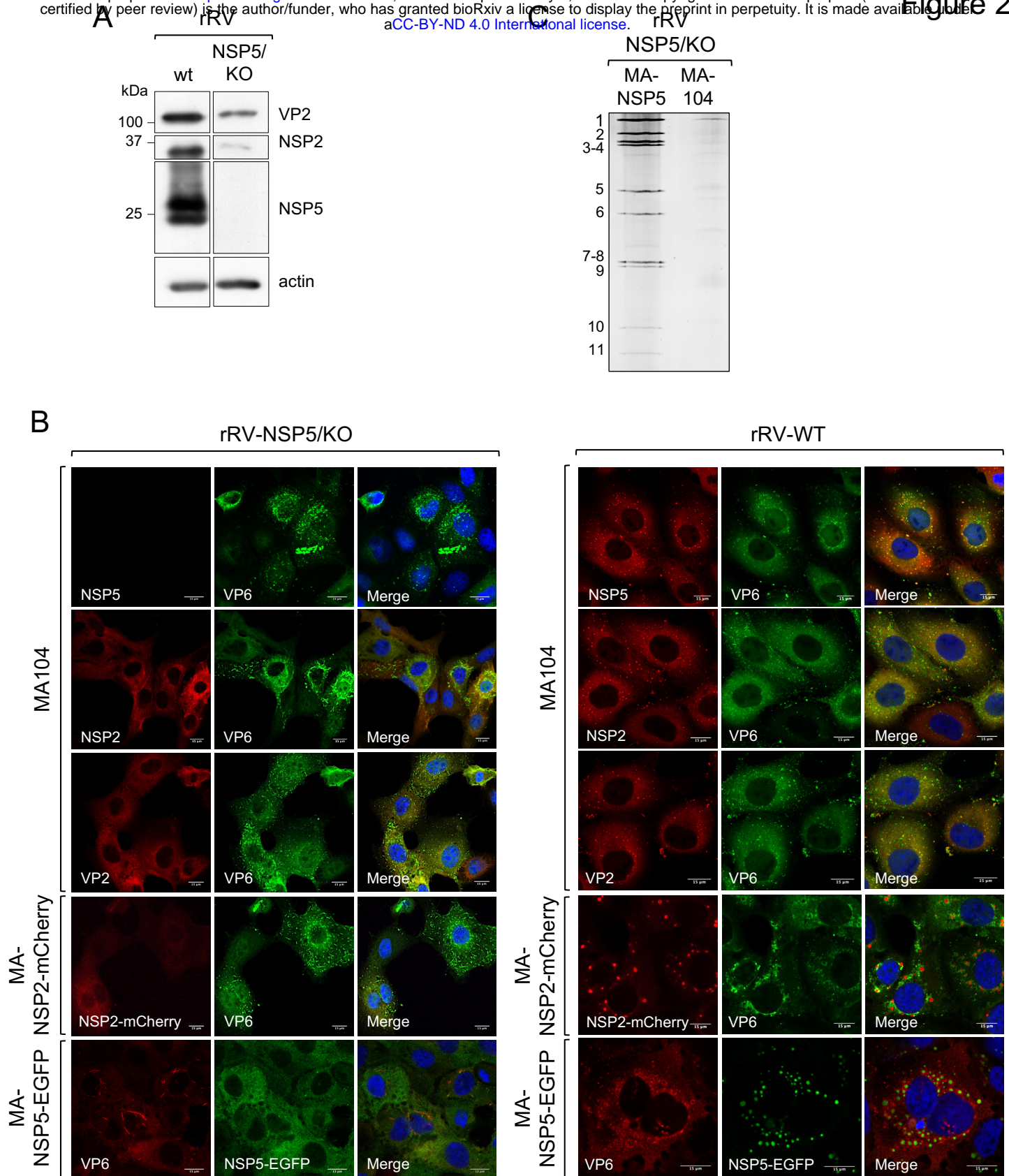
- 914 18. Campagna M, Marcos-Villar L, Arnoldi F, de la Cruz-Herrera CF, Gallego
915 P, Gonzalez-Santamaria J, Gonzalez D, Lopitz-Otsoa F, Rodriguez MS,
916 Burrone OR, Rivas C. 2013. Rotavirus Viroplasm Proteins Interact with the
917 Cellular SUMOylation System: Implications for Viroplasm-Like Structure
918 Formation. *J Virol* 87:807–817.
- 919 19. Afrikanova I, Miozzo MC, Giambiagi S, Burrone O. 1996. Phosphorylation
920 generates different forms of rotavirus NSP5. *J Gen Virol* 9:2059–2065.
- 921 20. Blackhall J, Fuentes A, Hansen K, Magnusson G. 1997. Serine protein
922 kinase activity associated with rotavirus phosphoprotein NSP5. *J Virol*
923 71:138–144.
- 924 21. Eichwald C, De Lorenzo G, Schraner EM, Papa G, Bollati M, Swuec P, de
925 Rosa M, Milani M, Mastrangelo E, Ackermann M, Burrone OR, Arnoldi F.
926 2018. Identification of a Small Molecule That Compromises the Structural
927 Integrity of Viroplasms and Rotavirus Double-Layered Particles. *J Virol* 92.
- 928 22. Contin R, Arnoldi F, Campagna M, Burrone OR. 2010. Rotavirus NSP5
929 orchestrates recruitment of viroplasmic proteins. *J Gen Virol* 7:1782–1793.
- 930 23. Afrikanova I, Fabbretti E, Miozzo MC, Burrone OR. 1998. Rotavirus NSP5
931 phosphorylation is up-regulated by interaction with NSP2. *J Gen Virol*
932 79:2679–2686.
- 933 24. Eichwald C, Jacob G, Muszynski B, Allende JE, Burrone OR. 2004.
934 Uncoupling substrate and activation functions of rotavirus NSP5:
935 phosphorylation of Ser-67 by casein kinase 1 is essential for
936 hyperphosphorylation. *Proc Natl Acad Sci U S A* 101:16304–16309.
- 937 25. Campagna M, Budini M, Arnoldi F, Desselberger U, Allende JE, Burrone
938 OR. 2007. Impaired hyperphosphorylation of rotavirus NSP5 in cells
939 depleted of casein kinase 1alpha is associated with the formation of
940 viroplasms with altered morphology and a moderate decrease in virus

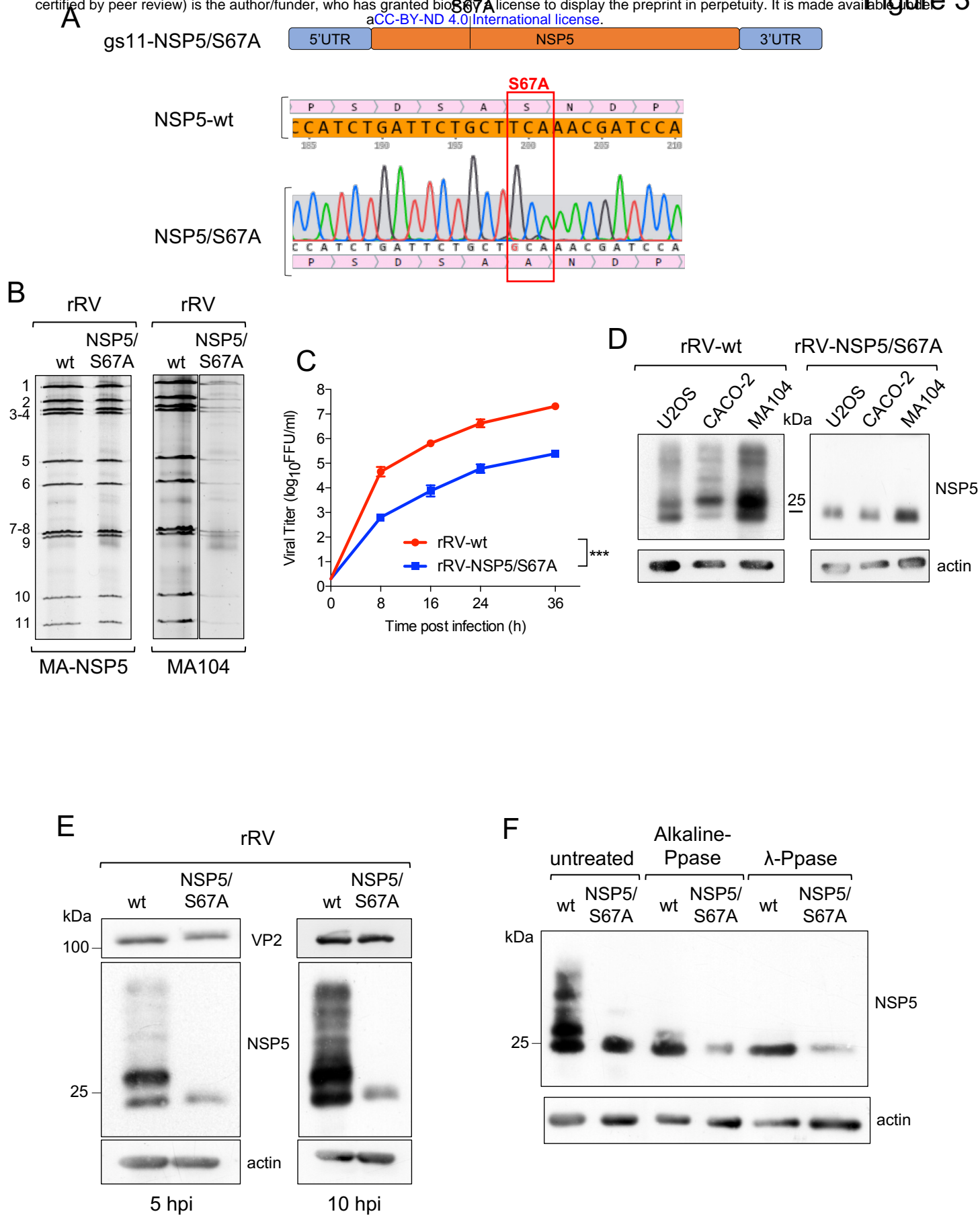
- 941 replication. *J Gen Virol* 10:2800–2810.
- 942 26. Eichwald C, Vascotto F, Fabbretti E, Burrone OR. 2002. Rotavirus NSP5:
943 mapping phosphorylation sites and kinase activation and viroplasm
944 localization domains. *J Virol* 76:3461–3470.
- 945 27. Martin D, Ouldali M, Menetrey J, Poncet D. 2011. Structural organisation of
946 the rotavirus nonstructural protein NSP5. *J Mol Biol* 413:209–221.
- 947 28. Kanai Y, Komoto S, Kawagishi T, Nouda R, Nagasawa N, Onishi M,
948 Matsuura Y, Taniguchi K, Kobayashi T. 2017. Entirely plasmid-based
949 reverse genetics system for rotaviruses. *Proc Natl Acad Sci U S A*
950 114:2349–2354.
- 951 29. Komoto S, Fukuda S, Ide T, Ito N, Sugiyama M, Yoshikawa T, Murata T,
952 Taniguchi K. 2018. Generation of Recombinant Rotaviruses Expressing
953 Fluorescent Proteins by Using an Optimized Reverse Genetics System. *J*
954 *Virol* 92:e00588-18.
- 955 30. Pertel T, Hausmann S, Morger D, Züger S, Guerra J, Lascano J, Reinhard
956 C, Santoni FA, Uchil PD, Chatel L, Bisiaux A, Albert ML, Strambio-De-
957 Castillia C, Mothes W, Pizzato M, Grütter MG, Luban J. 2011. TRIM5 is an
958 innate immune sensor for the retrovirus capsid lattice. *Nature* 472:361–
959 365.
- 960 31. Dull T, Zufferey R, Kelly M, Mandel RJ, Nguyen M, Trono D, Naldini L.
961 1998. A third-generation lentivirus vector with a conditional packaging
962 system. *J Virol* 72:8463–71.
- 963 32. Yusa K, Zhou L, Li MA, Bradley A, Craig NL. 2011. A hyperactive piggyBac
964 transposase for mammalian applications. *Proc Natl Acad Sci U S A*
965 108:1531–6.
- 966 33. Eichwald C, Arnoldi F, Laimbacher AS, Schraner EM, Fraefel C, Wild P,
967 Burrone OR, Ackermann M. 2012. Rotavirus viroplasm fusion and

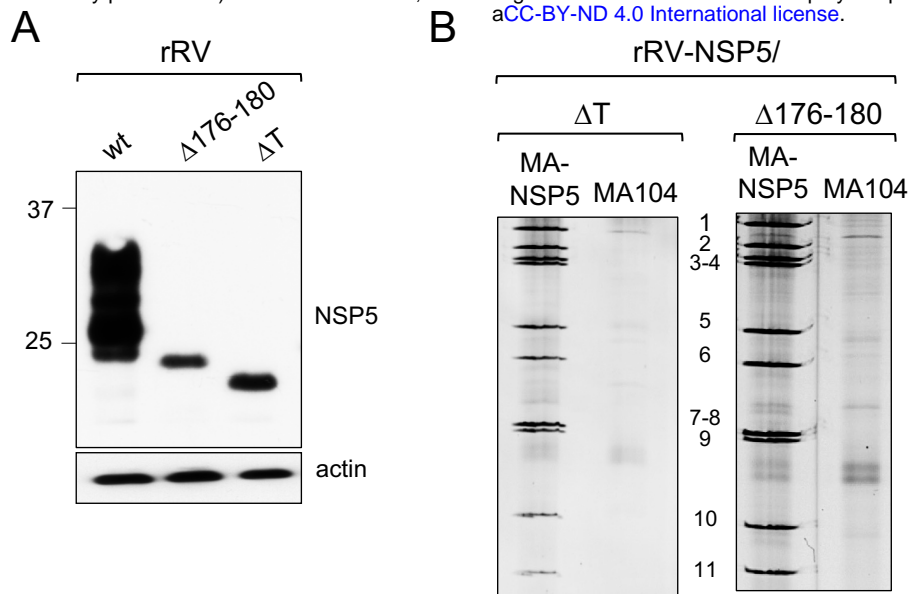
- 968 perinuclear localization are dynamic processes requiring stabilized
969 microtubules. *PLoS One* 7:e47947.
- 970 34. Vascotto F, Campagna M, Visintin M, Cattaneo A, Burrone OR. 2004.
971 Effects of intrabodies specific for rotavirus NSP5 during the virus replicative
972 cycle. *J Gen Virol* 85:3285–3290.
- 973 35. Ito H, Minamoto N, Goto H, Rong LT, Sugiyama M, Kinjo T. 1996.
974 Expression of the major inner capsid protein, VP6, of avian rotavirus in
975 mammalian cells. *Vet Microbiol* 49:257–65.
- 976 36. Tosser G, Labbé M, Brémont M, Cohen J. 1992. Expression of the major
977 capsid protein VP6 of group C rotavirus and synthesis of chimeric single-
978 shelled particles by using recombinant baculoviruses. *J Virol* 66:5825–31.
- 979 37. McDonald SM, Patton JT. 2011. Assortment and packaging of the
980 segmented rotavirus genome. *Trends Microbiol* 19:136–144.
- 981 38. Borodavka A, Desselberger U, Patton JT. 2018. Genome packaging in
982 multi-segmented dsRNA viruses: distinct mechanisms with similar
983 outcomes. *Curr Opin Virol* 33:106–112.
- 984 39. Criglar JM, Anish R, Hu L, Crawford SE, Sankaran B, Prasad BVV, Estes
985 MK. 2018. Phosphorylation cascade regulates the formation and
986 maturation of rotaviral replication factories. *Proc Natl Acad Sci*
987 115:E12015–E12023.
- 988 40. Liu C, Li Y, Semenov M, Han C, Baeg GH, Tan Y, Zhang Z, Lin X, He X.
989 2002. Control of beta-catenin phosphorylation/degradation by a dual-
990 kinase mechanism. *Cell* 108:837–47.
- 991 41. Amit S, Hatzubai A, Birman Y, Andersen JS, Ben-Shushan E, Mann M,
992 Ben-Neriah Y, Alkalay I. 2002. Axin-mediated CKI phosphorylation of β -
993 catenin at Ser 45: A molecular switch for the Wnt pathway. *Genes Dev.*

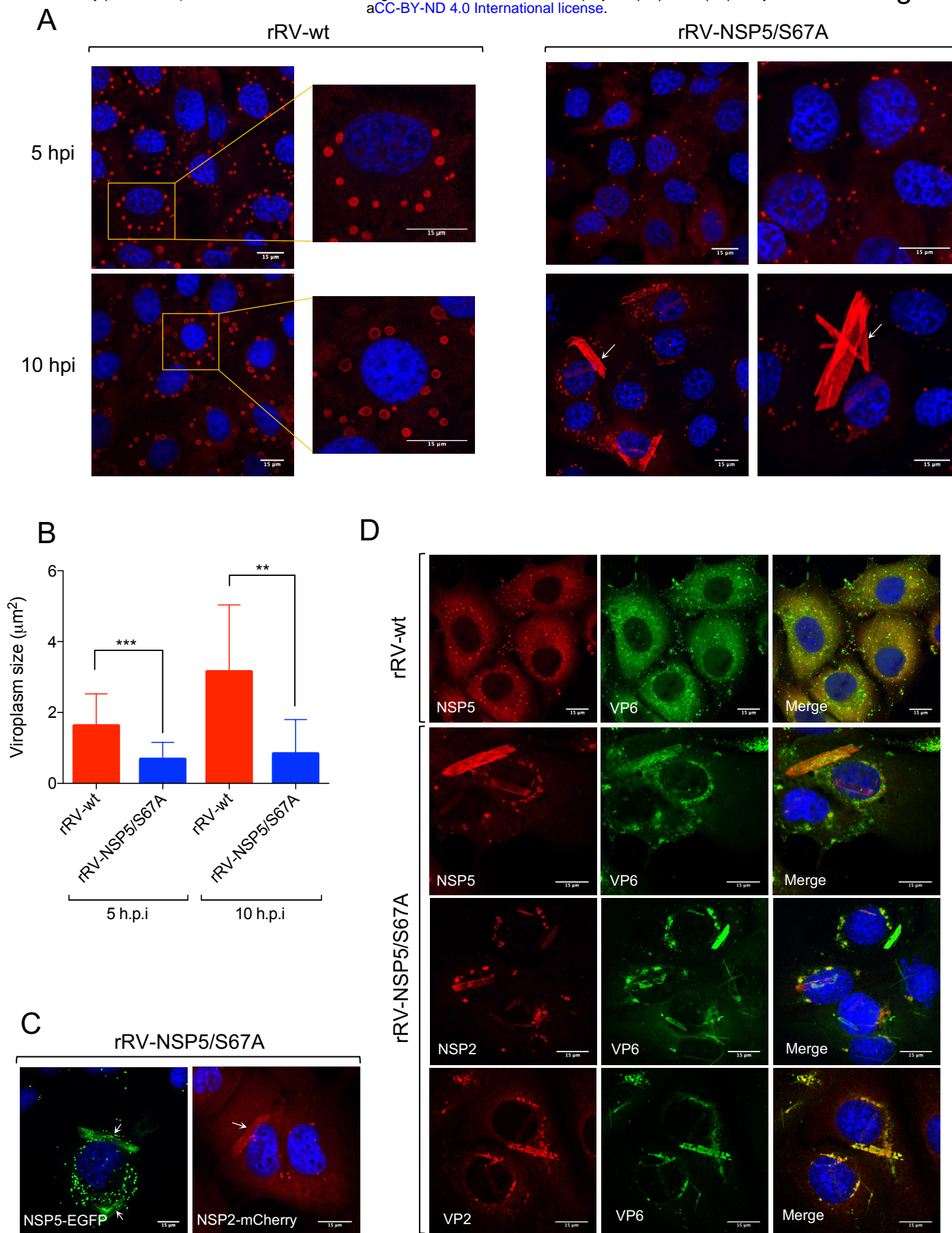
- 994 42. Verheyen EM, Gottardi CJ. 2010. Regulation of Wnt/ β -catenin signaling by
995 protein kinases. *Dev Dyn*.
- 996 43. Goonawardane N, Yin C, Harris M. 2018. A pivotal role of serine 225
997 phosphorylation in the function of hepatitis C virus NS5A revealed with the
998 application of a phosphopeptide antiserum and super-resolution
999 microscopy. *bioRxiv*.
- 1000 44. Kim J, Lee D, Choe J. 1999. Hepatitis C virus NS5A protein is
1001 phosphorylated by casein kinase II. *Biochem Biophys Res Commun*
1002 *257:777–781*.
- 1003 45. Ross-Thriepland D, Mankouri J, Harris M. 2015. Serine Phosphorylation of
1004 the Hepatitis C Virus NS5A Protein Controls the Establishment of
1005 Replication Complexes. *J Virol* *89:3123–3135*.
- 1006 46. Keating JA, Bhattacharya D, Lim P-Y, Falk S, Weisblum B, Bernard KA,
1007 Sharma M, Kuhn RJ, Striker R. 2013. West Nile virus methyltransferase
1008 domain interacts with protein kinase G. *Virology* *450:237–242*.
- 1009 47. Spencer K-A, Dee M, Britton P, Hiscox JA. 2008. Role of phosphorylation
1010 clusters in the biology of the coronavirus infectious bronchitis virus
1011 nucleocapsid protein. *Virology* *370:373–381*.
- 1012 48. Bhattacharya D, Hoover S, Falk SP, Weisblum B, Vestling M, Striker R.
1013 2008. Phosphorylation of yellow fever virus NS5 alters methyltransferase
1014 activity. *Virology* *380:276–284*.
- 1015





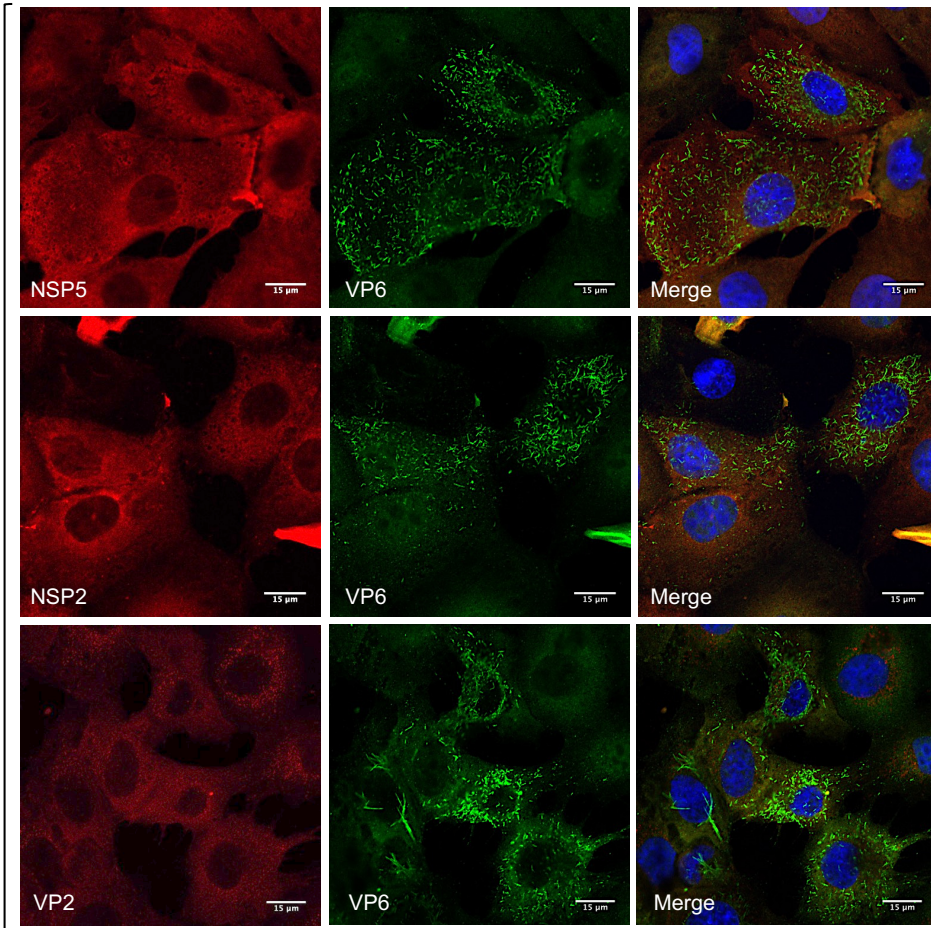






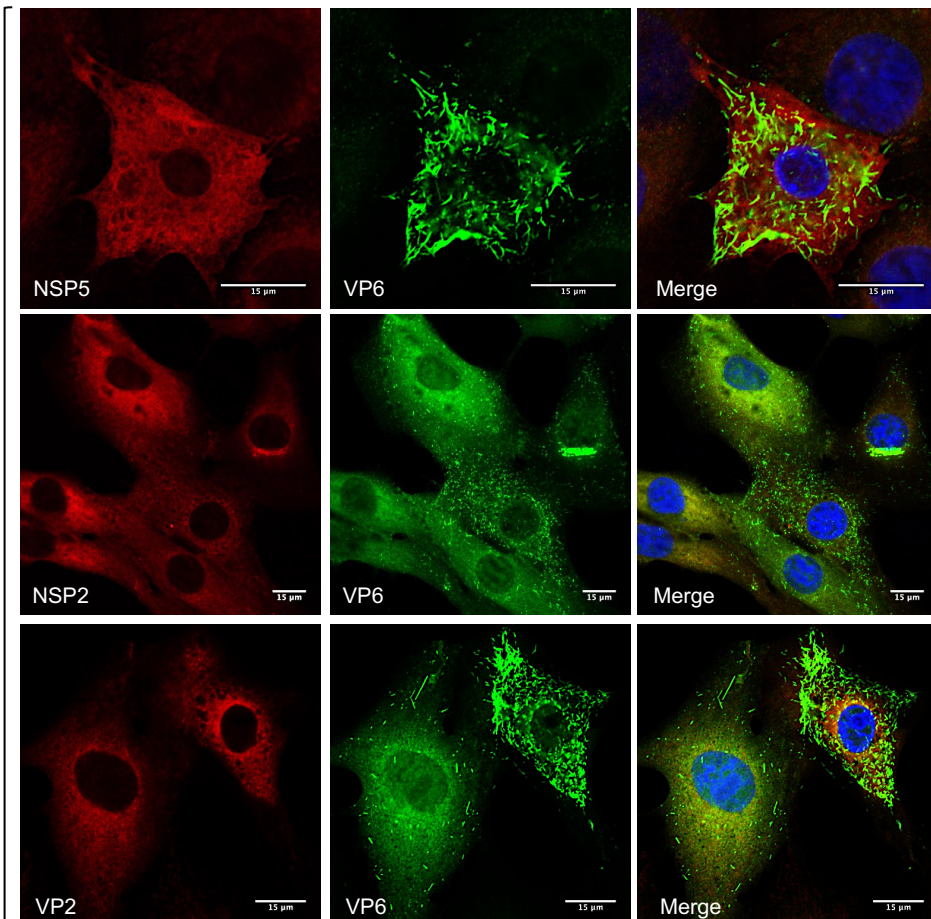
E

rRV-NSP5/ Δ 176-180

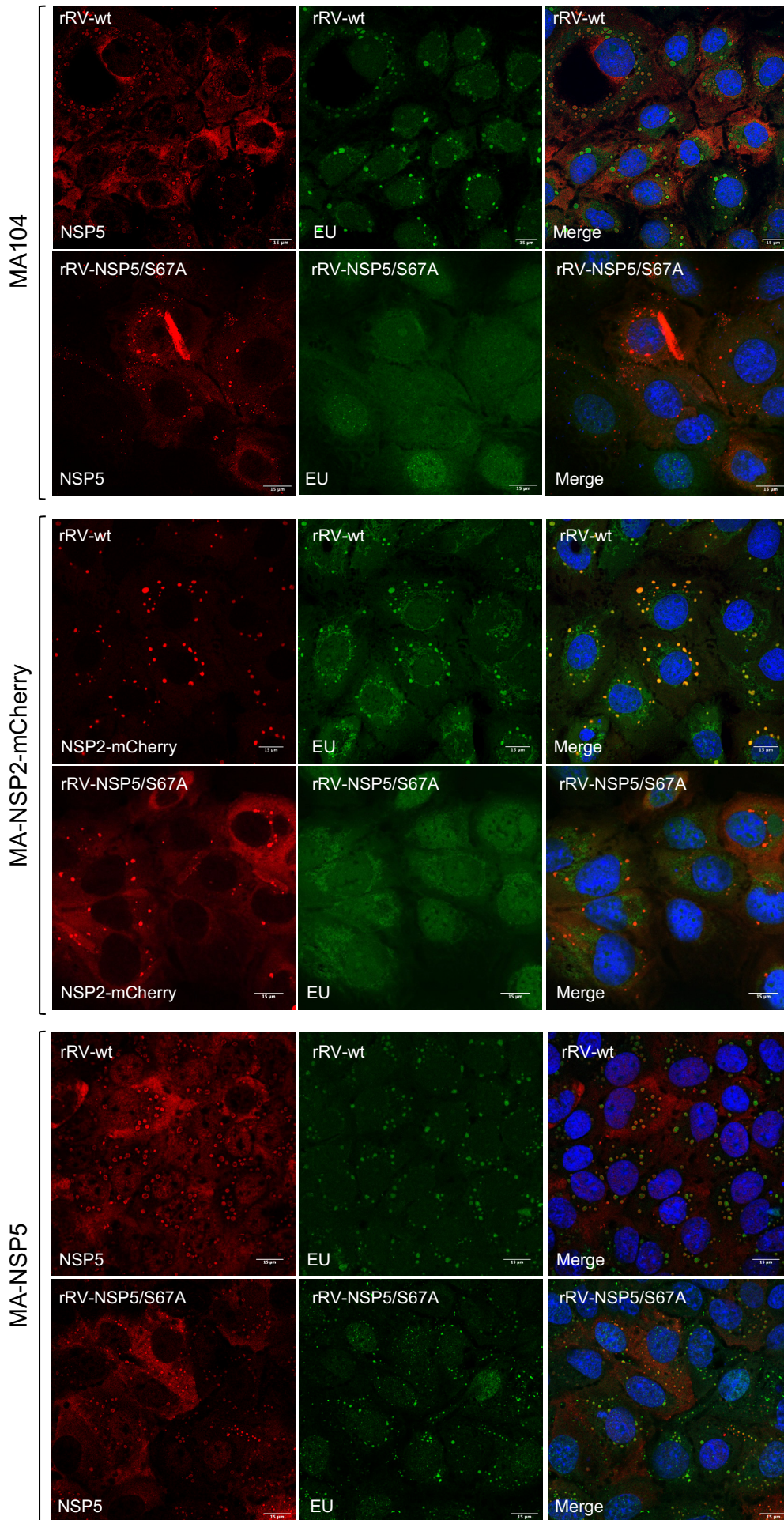


F

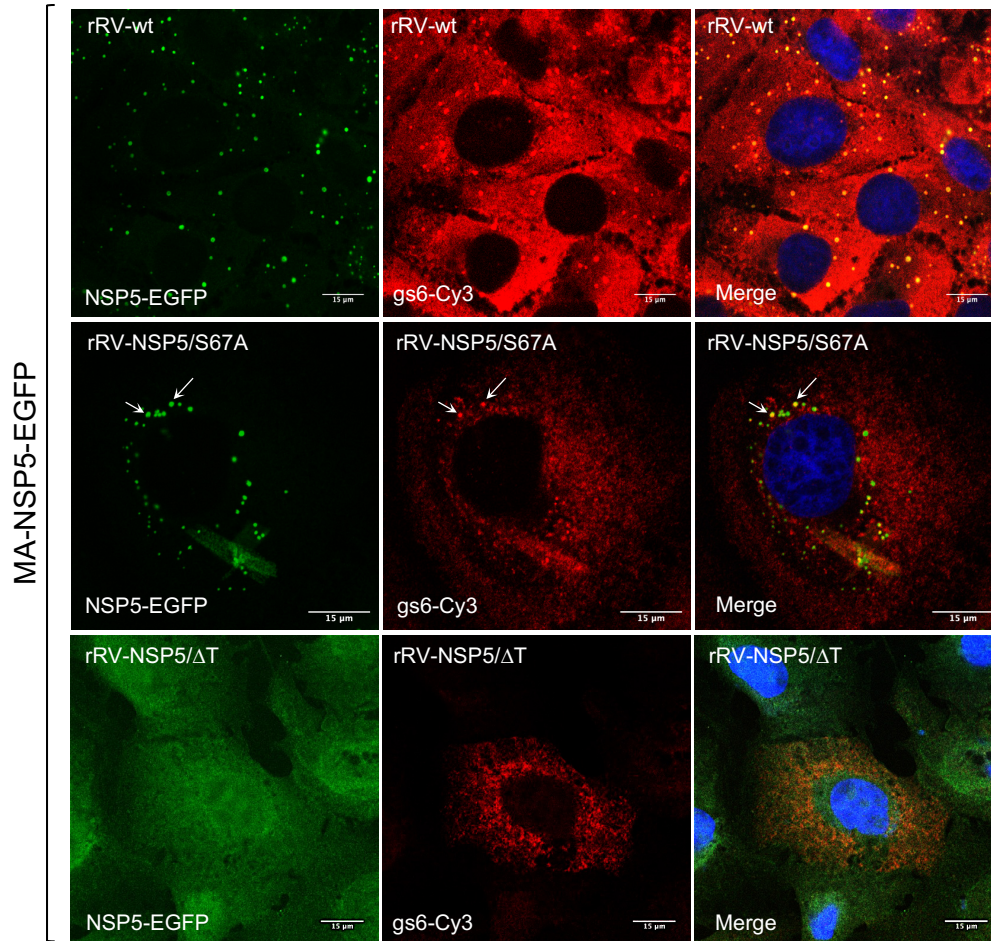
rRV-NSP5/ Δ T



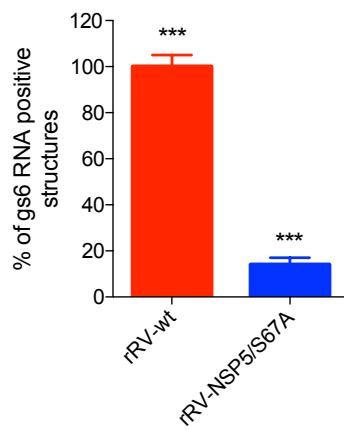
A

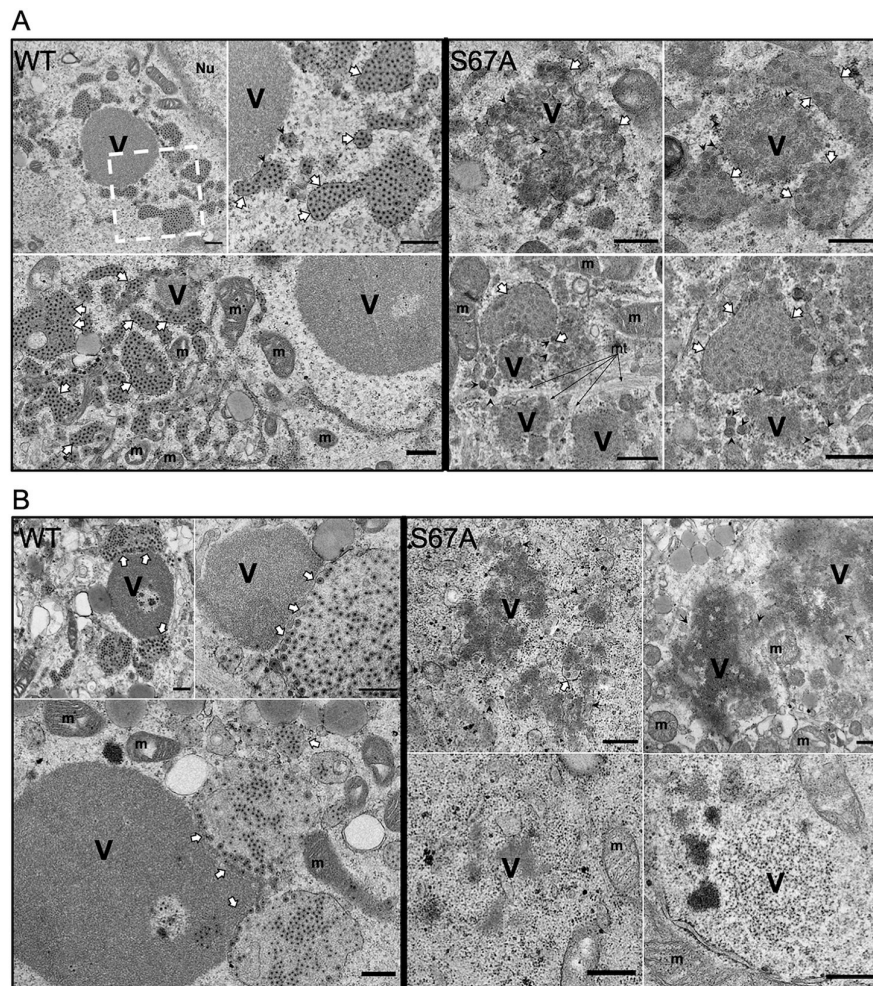


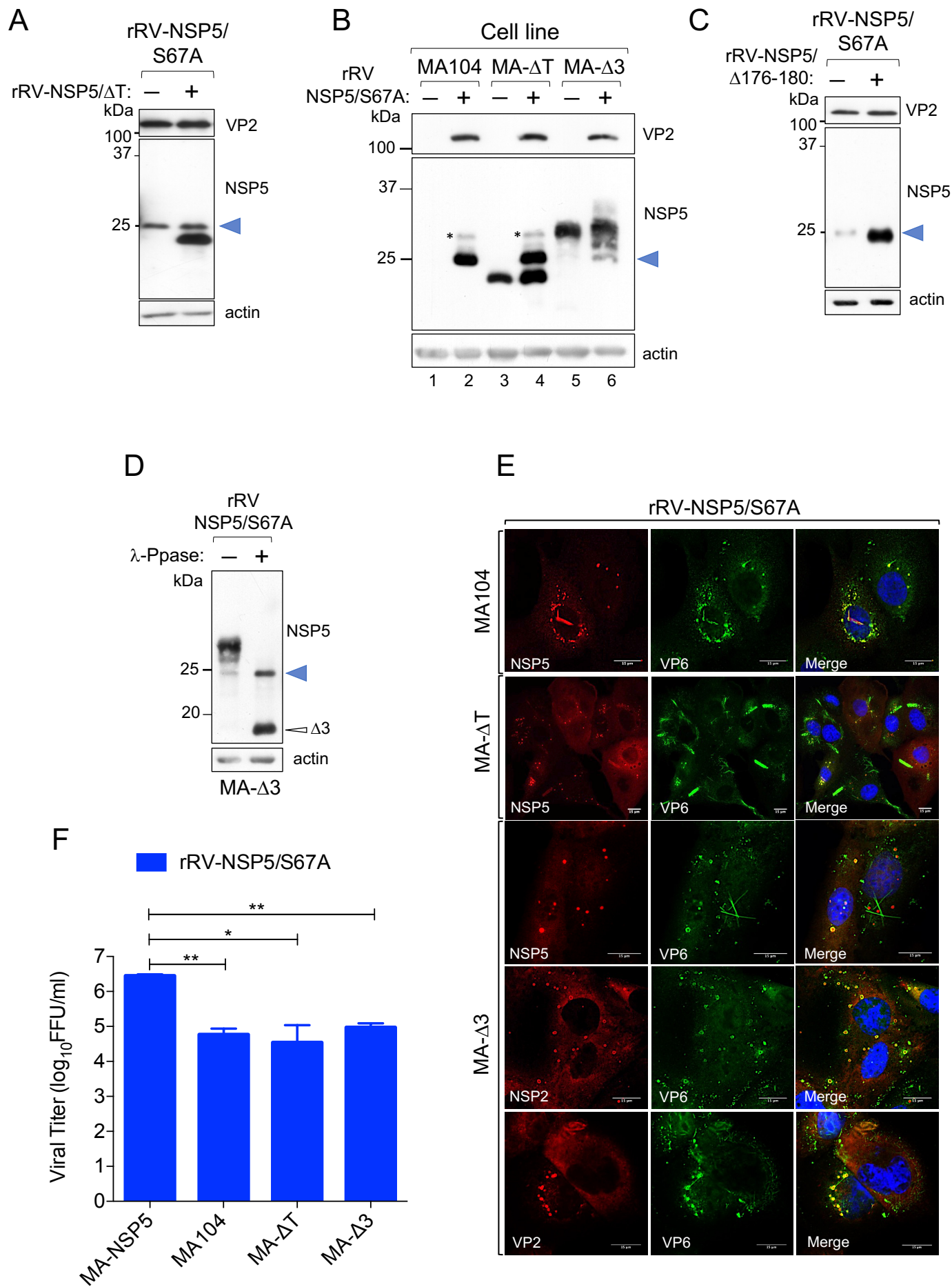
B

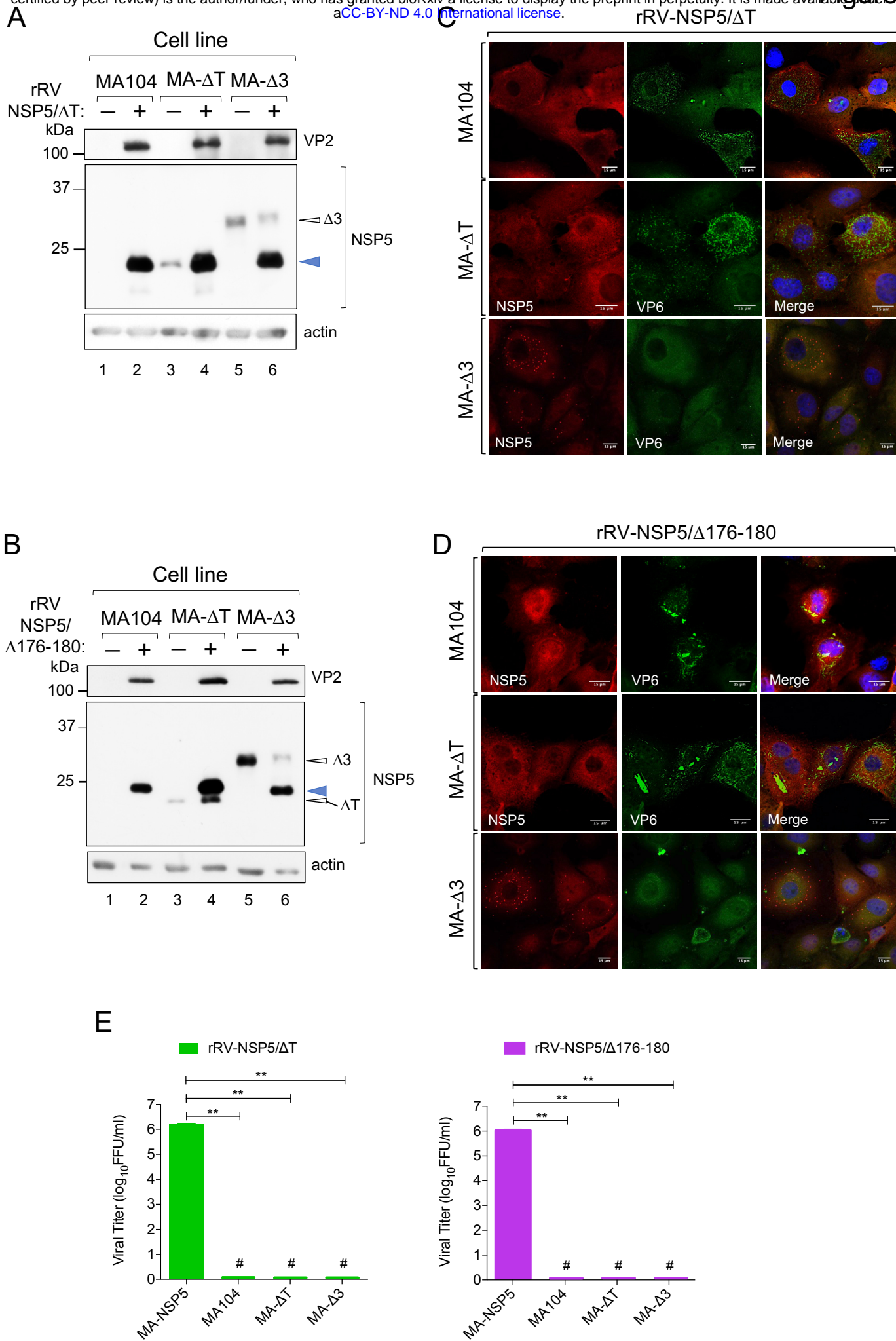


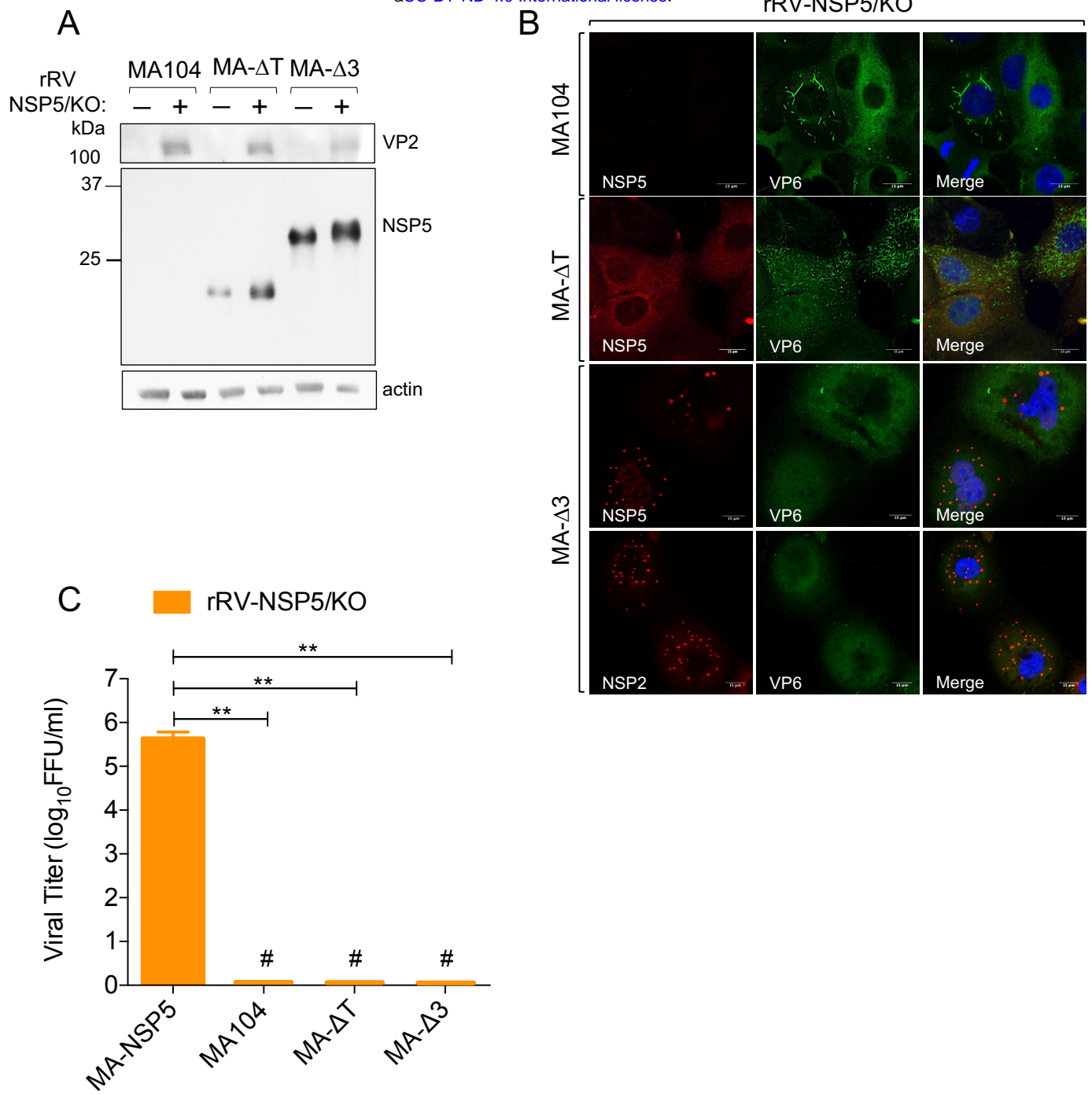
C

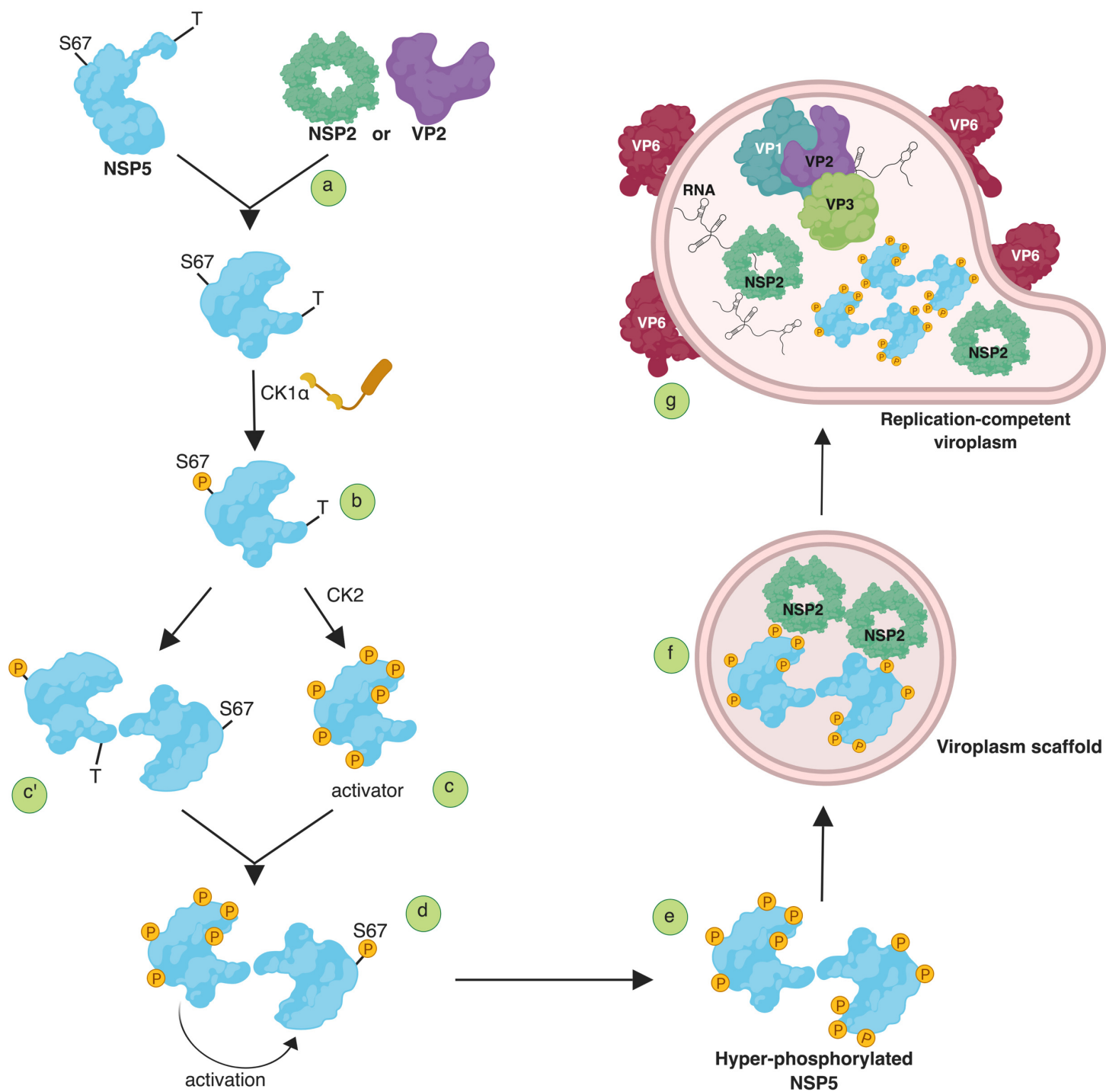


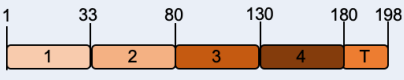


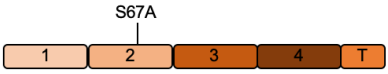

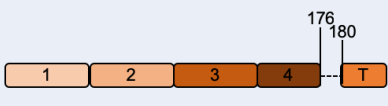

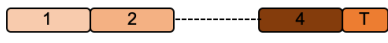
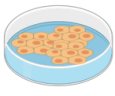



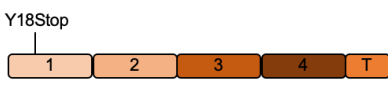




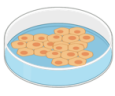










Construct	MA104 stable cell line	rRV
<p>NSP5 wt</p> 	 MA-NSP5	 rRV-wt
<p>NSP5/ S67A</p> 		 rRV-NSP5/S67A
<p>NSP5/ Δ176-180</p> 		 rRV-NSP5/ Δ 176-180
<p>NSP5/Δ3</p> 	 MA- Δ 3	
<p>NSP5/ΔT</p> 	 MA- Δ T	 rRV-NSP5/ Δ T
<p>NSP5/ KO</p> 		 rRV-NSP5/KO
<p>NSP5- EGFP</p> 	 MA-NSP5-EGFP	
<p>NSP2- mCherry</p> 	 MA-NSP2-mCherry	